



RESEARCH ARTICLE

10.1002/2015GC005980

Key Points:

- Bivalve shell horizons in deep-sea pockmarks are linked to past methane seepage
- A major seepage event persisted for ~1000 years between 17,707 and 16,689 years B.P.
- Shell bed formation is linked to structurally controlled seepage

Correspondence to:

W. G. Ambrose,
wambrose@bates.edu

Citation:

Ambrose, W. G. Jr., G. Panieri, A. Schneider, A. Plaza-Faverola, M. L. Carroll, E. K. L. Åström, W. L. Locke V, and J. Carroll (2015), Bivalve shell horizons in seafloor pockmarks of the last glacial-interglacial transition: a thousand years of methane emissions in the Arctic Ocean, *Geochem. Geophys. Geosyst.*, 16, doi:10.1002/2015GC005980.

Received 26 JUN 2015

Accepted 30 OCT 2015

Accepted article online 5 NOV 2015

Bivalve shell horizons in seafloor pockmarks of the last glacial-interglacial transition: a thousand years of methane emissions in the Arctic Ocean

William G. Ambrose Jr.^{1,2,3}, Giuliana Panieri¹, Andrea Schneider¹, Andrea Plaza-Faverola¹, Michael L. Carroll^{1,4}, Emmelie K. L. Åström¹, William L. Locke V², and JoLynn Carroll^{1,4}

¹Centre for Arctic Gas Hydrate, Environment and Climate, UiT-The Arctic University of Norway, Tromsø, Norway,

²Department of Biology, Bates College, Lewiston, Maine, USA, ³Now at Division of Polar Programs, National Science Foundation, Arlington, Virginia, USA, ⁴Akvaplan-niva, FRAM - High North Research Centre for Climate and the Environment, Tromsø, Norway

Abstract We studied discrete bivalve shell horizons in two gravity cores from seafloor pockmarks on the Vestnesa Ridge (~1200 m water depth) and western Svalbard (79°00' N, 06°55' W) to provide insight into the temporal and spatial dynamics of seabed methane seeps. The shell beds, dominated by two genera of the family Vesicomidae: *Phreagena* s.l. and *Isorropodon* sp., were 20–30 cm thick and centered at 250–400 cm deep in the cores. The carbon isotope composition of inorganic ($\delta^{13}\text{C}$ from -13.02‰ to $+2.36\text{‰}$) and organic ($\delta^{13}\text{C}$ from -29.28‰ to -21.33‰) shell material and a two-end member mixing model indicate that these taxa derived between 8% and 43% of their nutrition from chemosynthetic bacteria. In addition, negative $\delta^{13}\text{C}$ values for planktonic foraminifera (-6.7‰ to -3.1‰), concretions identified as methane-derived authigenic carbonates, and pyrite-encrusted fossil worm tubes at the shell horizons indicate a sustained paleo-methane seep environment. Combining sedimentation rates with ^{14}C ages for bivalve material from the shell horizons, we estimate the horizons persisted for about 1000 years between approximately 17,707 and 16,680 years B.P. (corrected). The seepage event over a 1000 year time interval was most likely associated with regional stress-related faulting and the subsequent release of overpressurized fluids.

1. Introduction

Methane hydrates are ice-like compounds that consist of gas molecules trapped inside water cages. Hydrates form on continental margins and in permafrost regions under low temperatures and high pressures [e.g., Sloan and Koh, 2008]. Methane reserves in the Arctic are unknown, but estimations range from ~100 to 600 metric Gt of carbon [Archer et al., 2009] with more than 95% of these reserves located in deep water [Ruppel, 2011]. The mechanisms responsible for triggering the release of methane from the seafloor vary depending on the geological setting. Shallow water hydrate deposits (depths less than ~400 m) have received considerable attention as these deposits are sensitive to ocean warming [e.g., Hunter et al., 2013; Graves et al., 2015]. As temperatures rise, the zone of gas hydrate stability (GHSZ) shallows until intercepting the seafloor, causing significant destabilization of gas hydrate deposits and the release of methane from the seafloor into the water column. If large quantities of methane gas are released from the seafloor and reach the atmosphere, hydrate destabilization may further exacerbate global atmospheric warming [Mienert et al., 2005; Westbrook et al., 2009; Berndt, 2014; Gentz et al., 2014; Sahling et al., 2014]. Deep-water methane hydrate provinces, where pressure has a dominant effect on hydrate stability [e.g., Dickens and Quinby-Hunt, 1994], require extended time scales for bottom water temperatures to warm sufficiently before destabilization will occur [Reagan and Moridis, 2007]. Marín-Moreno et al. [2013] predict that decades to centuries of ocean warming are required to generate methane emissions in water deeper than 420 m.

Methane emissions from gas hydrate provinces are a global phenomenon often recognized by the presence of seafloor morphologies (e.g., pockmarks and mounds) and acoustic flares [e.g., King and MacLean, 1970; MacDonald, 1990]. Identifying the processes controlling seepage distribution, periodicity, and duration in different hydrate provinces is necessary if we are to better understand the potential role of methane gas

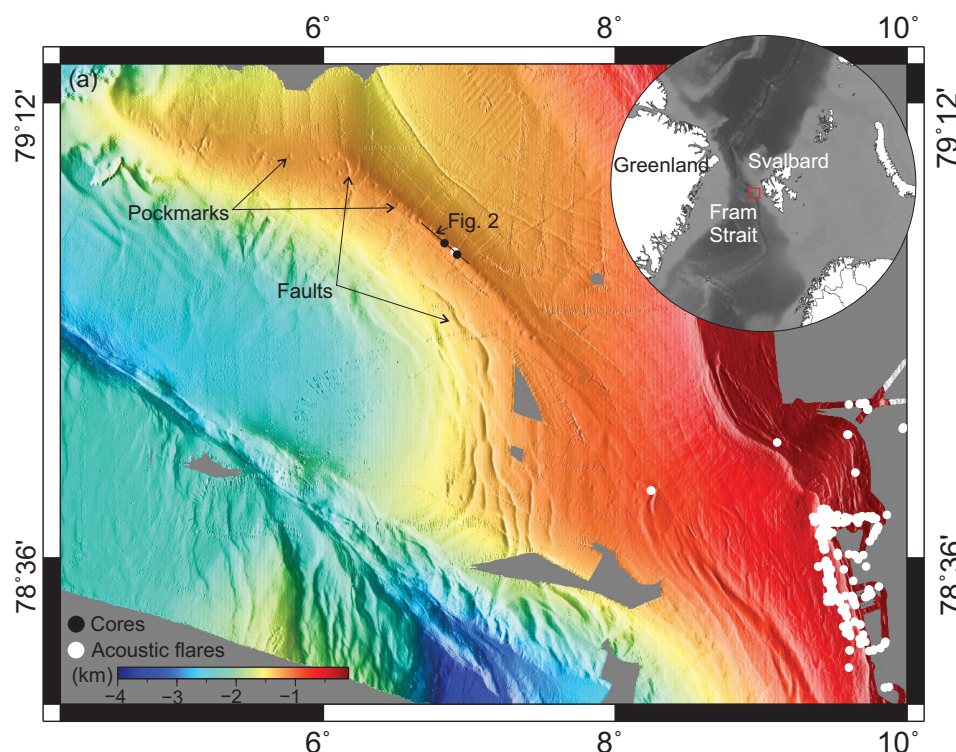


Figure 1. (a) High-resolution bathymetry (50×50 m) of the Vestnesa Ridge area and location of data samples as well as acoustic gas flares projected. The inset shows the location of Vestnesa Ridge in Fram Strait.

seepage on ocean chemistry and global climate. Vestnesa Ridge (Figure 1), at approximately 79°N lat., is one area where deep water methane emissions in the form of gas-bubble plumes and acoustic flares have been observed at water depths >1000 m [Bünz *et al.*, 2012; Hustoft *et al.*, 2009; Smith *et al.*, 2014]. This >100 km long ultraslow spreading ridge extends westward from the Spitsbergen continental margin, bounded by the Molloy Deep to the west, the Yermak plateau to the north and extending beyond the Molloy transform fault to the south. The methane hydrate system at Vestnesa is a reservoir of long-lived gas hydrate and free gas of a mixed origin: microbial, thermogenic, and abiogenic [Johnson *et al.*, 2015]. Sets of buried mounds and pockmarks exist along the entire extent of Vestnesa Ridge, indicating regular seepage periods. Presently, seepage is occurring toward the eastern segment of the ridge.

Hydrothermal vents and hydrocarbon seeps have been characterized as deep-sea biological oases that support chemosynthetic-based communities with high diversity, biomass, and carbon cycling [Van Dover, 2000; Levin, 2005; Vanreusel *et al.*, 2009; Thurber *et al.*, 2013]. Hydrothermal vents discharge methane, hydrogen sulfide, and mineral-rich hydrothermal fluid with temperatures up to 400°C . Hydrocarbon seeps involve the upward seepage of methane dissolved in water or as small bubbles, hydrogen sulfide, or other hydrocarbon-rich fluids at temperatures that are only slightly elevated above ambient seawater. The principal chemosynthesis-dependent bivalve families that have been discovered at vents and seeps are Vesicomidae, Thyasiridae, Lucinidae, Mytilidae, and Solemididae [Taylor and Glover, 2010]. The Vesicomidae occur at most known vents and seeps where they are often the most abundant macrofaunal taxa [Krylova and Sahling, 2010]. They derive their energy from symbiotic sulfur-oxidizing bacteria housed in their gills [Cavanaugh, 1983; Decker *et al.*, 2013] and can reach densities of over 1000 individuals and biomass of 30 kg wet weight per m^2 [Alexis *et al.*, 2015, and references therein]. The best studied methane seep community in the Arctic is the Håkon Mosby Mud Volcano south of Svalbard (1280 m depth) [Niemann *et al.*, 2006; Vanreusel *et al.*, 2009] and gas flare sites offshore western Svalbard (90–387 m water depth) [Sahling *et al.*, 2014].

Chemosynthetic-based communities supported by methane seeps are also well recognized in the geological record. Although present as early as the Proterozoic [Campbell, 2006; Kiel and Little, 2006; Kiel, 2010;

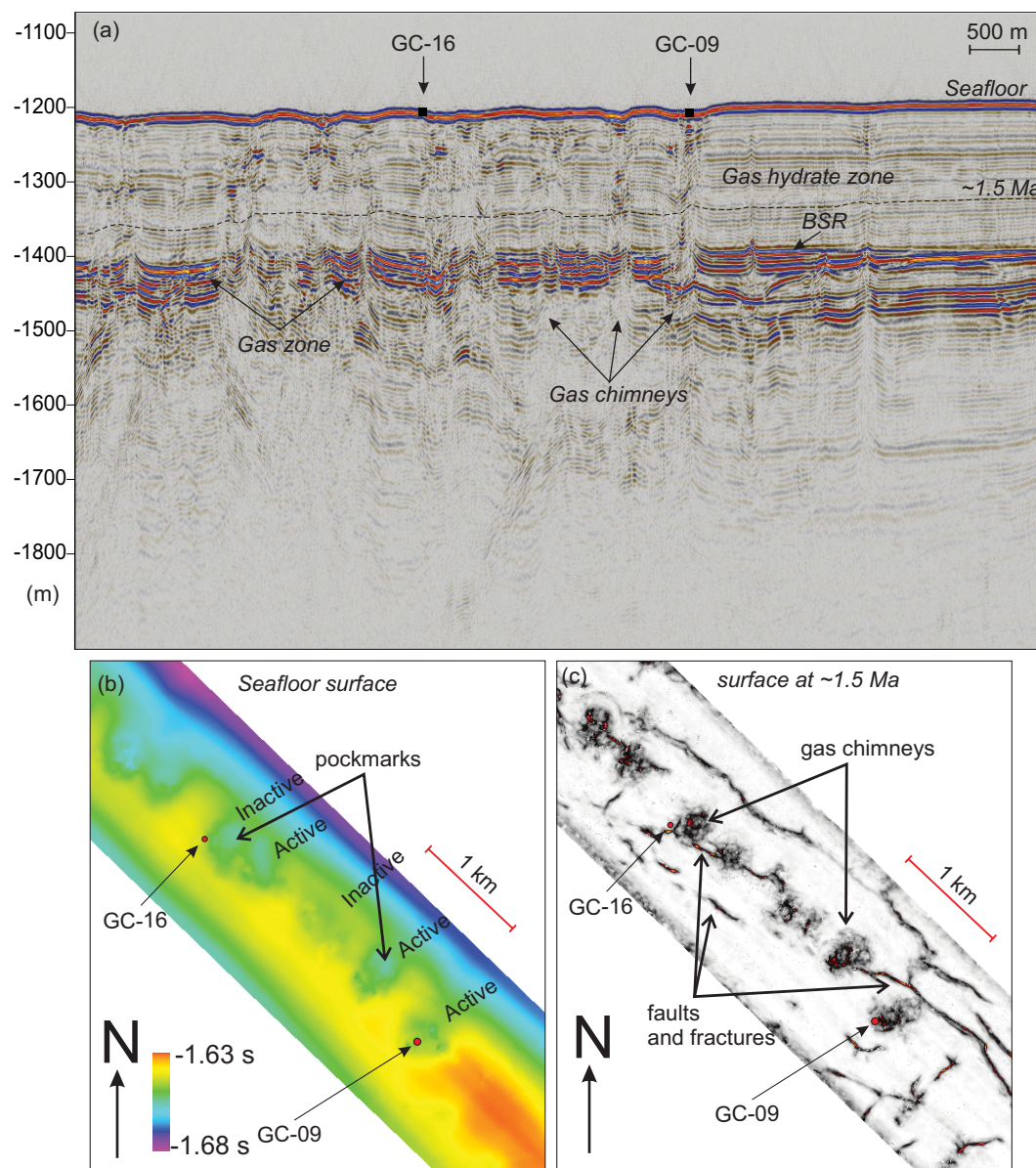


Figure 2. (a) High-resolution 2-D P-Cable seismic profile converted to depth, showing fluid-flow-related structures underlying seafloor pockmarks at the location of the investigated samples; (b) seafloor map from high-resolution 3-D P-Cable seismic data showing the morphology of pockmarks associated with active and relict seepage on Vestnesa Ridge; (c) subseabed structural map modified after Plaza-Faverola *et al.* [2015], extracted along a horizon estimated to be ~1.5 Ma old. Pockmarks and associated gas chimneys are in close proximity of faults and fractures. The locations of the gravity cores are noted (red dots).

Taviani *et al.*, 2011], seeps dominated by vesicomid and lucinid bivalves do not appear until the Cenozoic [Callander and Powell, 2000, and references therein]. Dense assemblages of fossil bivalves in deep-sea sediments have been used to identify fossil seeps [Campbell and Bottjer, 1995; Majima *et al.*, 2005; Chien *et al.*, 2012; Amano *et al.*, 2013]. The chemical and mineral content of shells provides a record of environmental conditions during the life of the individual [Torres *et al.*, 2001; Hein *et al.*, 2006; Mae *et al.*, 2007; Lietard and Pierre, 2008, 2009; Lartaud *et al.*, 2010; Han *et al.*, 2014], thereby providing insight into seep dynamics.

Two discrete bivalve shell horizons (hereafter termed “shell beds”), one in each of two gravity cores (HH-13-203 GC09; HH-13-211 GC16), recovered from the Vestnesa Ridge in 2013 [Mienert, 2013] became apparent after the cores were X-rayed. Both cores are from pockmarks at water depths of about 1200 m, one of them collected at a site exhibiting active gas flares (Figures 1 and 2). We focus on these deep-sea shell beds in the Arctic: first to confirm that the bivalves were associated with methane seeps, second to describe the

physical and biological conditions supporting this bivalve community, and finally to use the shell beds as a paleoproxy to reconstruct the duration and timing of Arctic methane emission at Vestnesa Ridge. We used bivalve shell chemistry, carbonate chemistry of associated foraminifera, coupled with sediment and carbonate mineralogy, as evidence for chemosynthesis-based seep communities. Our study provides new insights into the mechanisms controlling the temporal pattern of methane emissions at a deep water hydrate system, namely the Vestnesa Ridge.

2. Methods

2.1. Core Collection and Initial Preparation

Sediment gravity core HH-13-203 GC09 (79°00.143977N, 06°55.683059E; 300 cm recovered) was collected from a pockmark with an active gas flare on the Vestnesa Ridge at a water depth of 1210 m on 13 October 2013 (Figure 2). The second gravity core HH-13-211 GC16 (79°01.86696N, 06°49.850833E; 498 cm recovered) was collected on 14 October 2013 approximately 6 km to the south in a water depth of 1202 m. Both cores were collected from pockmarks, but the location of core HH-13-211 GC16 showed no evidence of gas emission at the time of sampling. For the remainder of this paper, sediment gravity core HH-13-203 GC09 is designated as GC09 and sediment gravity core HH-13-211 GC16 is designated as GC16.

Upon recovery, sediment cores were sectioned into ~100 cm sections and kept cool at ~5°C. Before opening the core onshore, magnetic susceptibility was measured with a Bartington MS2 loop sensor; afterward the core was cut lengthwise. One core half was archived after being X-rayed (Geotek MSCL-XCT) and imaged with a JAI L-107CC 3 CCD RGB line scan camera on an Avaatech XRF core scanner. The working half was sampled at different depth intervals. Samples of ~1 cm thick were sampled for shell material and micropaleontology. Individual sediment samples were weighed, freeze-dried, re-weighed, and then soaked in distilled water. The samples were then wet sieved with mesh widths of 63 μm and the residues dried at 30°C. The samples were subsequently sieved using mesh widths of 100 and 500 μm . Bivalve shells and fragments (>1 mm in length) were removed from the material retained on the 100 μm sieve and weighed to the nearest 0.001 g. The >63 and >100 μm dry residues were examined for benthic and planktonic foraminifera.

2.2. Analytical Methods

2.2.1. Bivalve Sample Preparation

We focused our sampling on the bivalve-rich core sections and on areas immediately above and below them (see Figures 3 and 4 with descriptions given in section 3.1). Large bivalve shells were removed from the core sections prior to sectioning into ~1 cm thick samples.

Shell material to be used for stable isotopic analysis was first treated with hydrogen peroxide (30% for 24 h) [Hein *et al.*, 2006] in order to remove the periostracum and any other organic material on the shell surface. The material was then rinsed with deionized water, air-dried, and examined under a microscope for any surface evidence of diagenesis, such as carbonate overgrowth. Following this cleaning procedure, samples were milled using a DREMEL tool with a 1.5 mm bur. The shell powder obtained by milling was collected for mineral analysis (X-ray diffraction) and stable isotope analysis ($\delta^{18}\text{O}$, $\delta^{13}\text{C}$).

We performed X-ray diffraction (XRD) on subsamples of the milled shell powder in order to determine whether the composition of the shell was aragonite or calcite and, if both were present, the proportion of each in the shell [Hein *et al.*, 2006]. XRD was performed using a Rigaku Miniflex II Desktop X-Ray Defractometer. Minerals were identified and quantified (percent) using MDI Jade 9 software.

As an additional check for evidence of diagenesis, two large shell fragments from GC09 and four shell fragments from GC16 were cut in half, and one half was treated with acetic acid (25%, 15 min) [Hein *et al.*, 2006]. This treatment allows us to evaluate the possible presence of unseen authigenic aragonite on the stable carbon isotope ratio in the inorganic portion of the shell, though this treatment would not of course account for any authigenic calcite precipitation.

The calcium carbonate matrix of shells also contains organic carbon in the form of the scleroprotein or conchiolin, which is a reflection of the animal's diet [O'Donnell *et al.*, 2003; Mae *et al.*, 2007; Dreier *et al.*, 2014]. We extracted the shell organics from the inorganic shell material, first placing 7.5–13.5 mg of shell powder into methanol rinsed silver capsules. Capsules were then placed in a Teflon block within a dry bath. Dry

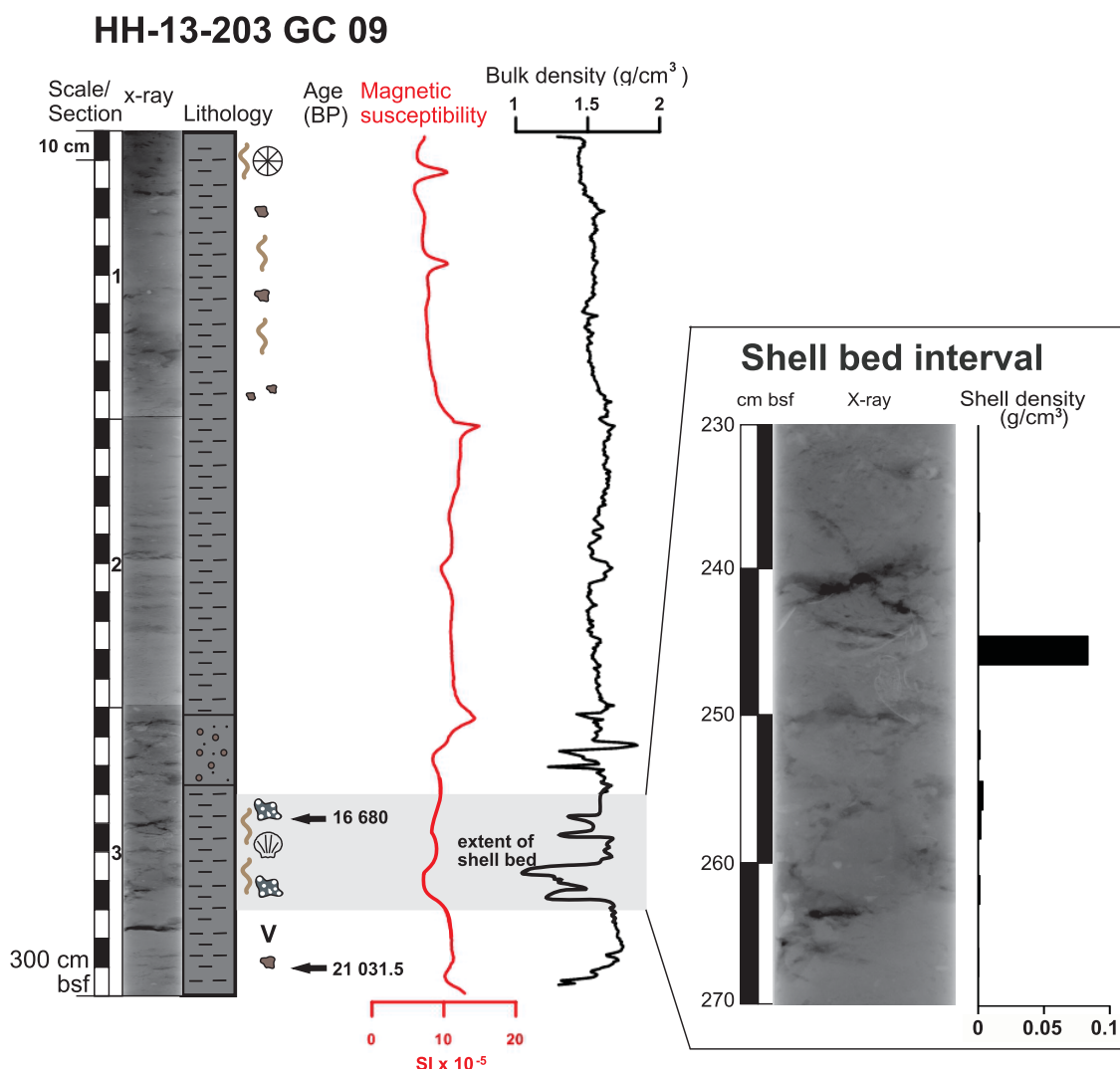


Figure 3. X-ray images, visual description of the lithology, magnetic susceptibility, and bulk density from GC09. Close-up of X-ray and shell density (g shell/cm³ of sediment) for the shell bed interval (236–268 cm). GC09 was 300 cm long, but the Holocene deposit at the top was missing. Legend in Figure 4.

bath heat was set to maintain 65–70°C, 0.1 N hydrochloric acid was immediately added to each capsule 10 μL at a time, waiting between further additions until reaction visibly ceased and gradually increasing acid additions to 20, 30, and finally 50 μL until a total addition of 350 μL was achieved. Samples were left in a dry bath 6–24 h until dry.

2.2.2. Bivalve Stable Isotope Analysis

Both the inorganic and organic sample fractions were analyzed for stable carbon isotopes ($\delta^{13}\text{C}_{\text{inorganic}}$, $\delta^{13}\text{C}_{\text{organic}}$) using the elemental analyzer-combustion interface-stable isotope ratio mass spectrometer at the Environmental Geochemistry Laboratory (Bates College, Maine, USA). For the inorganic fraction, sample sizes of powdered shell were 0.4–0.6 mg. We also analyzed shell samples of *Serripes groenlandicus*, a shallow water suspension-feeding bivalve common to the Barents and Greenland Seas [Carroll *et al.*, 2011], as a modern control to make sure we successfully removed all inorganic material prior to measuring the isotopic composition of shell organics. Isotopic values are expressed in delta (δ) notation as per mil (‰) enrichment relative to international standards. The standard for carbon and nitrogen is Vienna Pee Dee Belemnite (VPDB) [Craig, 1957] and air, respectively. Internal standards were run every eight samples. The reproducibility was $\pm 0.2\text{‰}$.

Analysis of shell powder for $\delta^{18}\text{O}$ with $\delta^{13}\text{C}$ was performed at the Department of Geological and Atmospheric Sciences, Iowa State University, USA. Samples were analyzed using a Finnigan Delta Plus XL mass

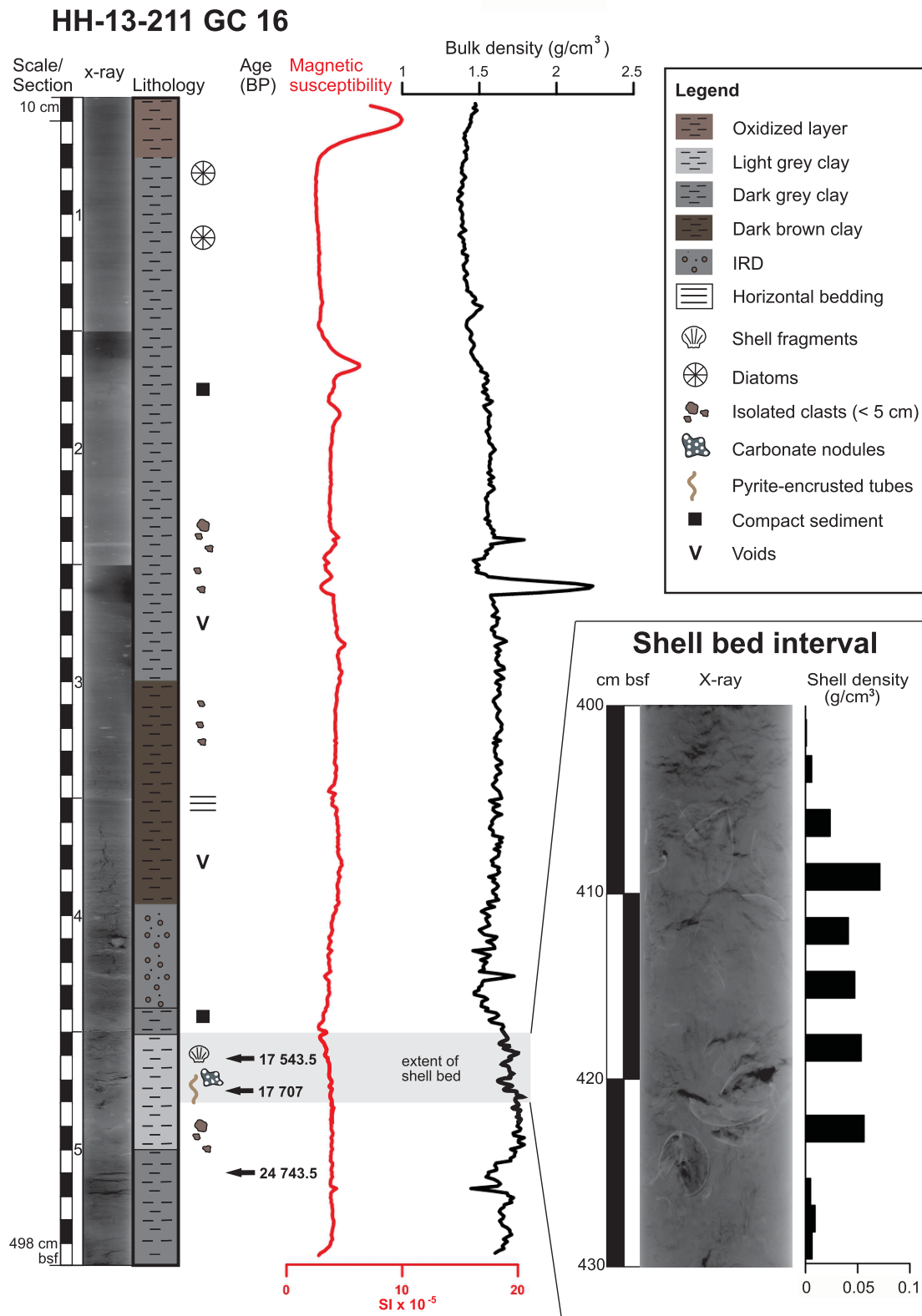


Figure 4. X-ray images, visual description of the lithology, mass-specific magnetic susceptibility, bulk density from core GC16. Close-up of X-ray and shell density ($g\ shell/cm^3$ of sediment) for the shell bed interval (400–430 cm).

Table 1. AMS ^{14}C Dating Results of Bivalve Shells (B) and Planktonic Foraminifera (Pf)^a

Core	Depth Below Surface (cm)	Laboratory Code	Taxon	Uncorrected AMS ^{14}C Age	ΔR	Corrected Age (2σ) (^{14}C kyr B.P.)	Mean Corrected Age (2σ) (^{14}C kyr B.P.)	$\delta^{13}\text{C}$ (‰)
GC16	395.5	Beta-397277	Pf	17,340 ± 60	7 ± 11	18,655–18,241	20,398	−3.70
GC16	414.5	Beta-397278	Pf	17,440 ± 60	7 ± 11	18,778–18,370	20,524	−3.10
GC16 ^b	414.5	Beta-397280	B	14,840 ± 50	65 ± 37	15,796–15,391	17,543.5	0.90
GC16 ^b	423.5	Beta-397281	B	14,960 ± 50	65 ± 37	15,946–15,568	17,707	0.10
GC16 ^b	460.5	Beta-397279	Pf	20,960 ± 70	7 ± 11	23,106–22,481	24,743.5	−1.60
GC09	230.5	Beta-397274	Pf	16,550 ± 50	7 ± 11	17,689–17,320	19,454.5	−5.10
GC09 ^b	237.0	Beta-397282	B	14,230 ± 50	65 ± 37	14,980–14,480	16,680	−7.90
GC09	237.0	Beta-397275	Pf	17,110 ± 50	7 ± 11	18,388–18,002	20,145	−6.70
GC09	270.5	Beta-397276	Pf	18,170 ± 60	7 ± 11	19,810–19,305	21,507.5	−5.60
GC09 ^b	290.5	Beta-408804	Pf	17,830 ± 50	7 ± 11	19,297–18,866	21,031.5	−1.20

^aCalibrated dates are presented in kyr B.P. A regional correction of $\Delta R = 7 \pm 11$ years was applied for planktonic foraminifera and $\Delta R = 65 \pm 37$ for the bivalve shells, following the recommendations of Mangerud and Gulliksen [1975]. The final ages were calculated as the mean from the calibrated age range with a standard deviation of 2σ . $\delta^{13}\text{C}$ values relative are to the Vienna Pee Dee Belemnite (VPDB).

^bData were used for dating.

spectrometer in continuous flow mode connected to a gas bench. Reference samples were run after every five samples.

2.2.3. Micropaleontology

Samples for benthic and planktonic foraminifera were semiquantitatively analyzed in every 2 cm interval within the shell bed and every 10 cm interval in the remainder of the core. A total of 33 samples from GC16 and 25 samples from GC09 were selected for micropaleontological analysis. Planktonic and benthic foraminifera were identified largely following the taxonomy of Hembleben *et al.* [1989] and Loeblich and Tappan [1987], respectively. Special attention was paid to the state of preservation of foraminifera since the shell wall can be affected by secondary carbonate precipitation in the presence of methane seepage. Selected specimens of all taxa were mounted onto microslides to provide a permanent record and for identification purposes. Some specimens were selected for scanning electron microscopy SEM. All residues, specimens and images are stored at the Department of Geology, at UiT—the Arctic University of Norway, Tromsø.

2.2.4. ^{14}C Dating

Ten ^{14}C AMS (Accelerator Mass Spectrometry) dates were performed on monospecific samples of planktonic foraminifera (*N. pachyderma* (s)) and individual whole shells at the Beta Analytic Inc., Miami, Florida, USA (Table 1). We analyzed only *N. pachyderma* (s) and bivalve samples that exhibited a good state of preservation to minimize the likelihood of chronological inconsistencies resulting from secondary diagenesis. We rejected samples that showed visual evidence of mineralogical alteration or broken specimens. Samples with $\delta^{13}\text{C}$ values exceeding negative 1.60‰ were disregarded since a negative $\delta^{13}\text{C}$ value is evidence of incorporation of methane-derived carbon into the AMS ^{14}C . This would result in ^{14}C ages that are too old.

The radiocarbon dates were calibrated to calendar years using the Calib 7.1 program [Stuiver *et al.*, 2014] and the marine calibration curve Marine13 [Reimer *et al.*, 2013] that operates with a standard reservoir correction of −400 years [Mangerud and Gulliksen, 1975]. We applied a regional correction of $\Delta R = 7 \pm 11$ years, following the recommendations for planktonic foraminiferal dates by Bondevik and Gulliksen in Mangerud *et al.* [2006]. For bivalve shells, we used a regional correction of 65 ± 37 years [Mangerud and Gulliksen, 1975]. The ages were calculated as the midpoint value from the calibrated age range ($\pm 2\sigma$). Calibrated dates are presented in years before present (B.P.) A.D. 1950 with standard deviation 2σ .

2.2.5. Mineralogy and Geochemistry

Scanning electron microscope (Hitachi SEM Tabletop) observations were made on samples of carbonate clasts between 474 and 498 cm, and acicular aragonite from 457 to 498 cm of GC09 (Figures 3 and 5). We analyzed samples of pyrite and carbonate clasts retrieved from sediments in the upper meter of GC16 and between 250 and 260 cm (Figures 4 and 5). We also characterized the morphologies and chemical compositions of these samples by energy dispersive X-ray spectroscopy (EDAX, Bruker Nano GmbH).

Analysis of two carbonate nodules (from 245 cm in GC09 and from 428 cm in GC16) for $\delta^{18}\text{O}$ with $\delta^{13}\text{C}$ was performed with a ThermoFinnigan MAT252 mass spectrometer coupled with CarboKiel-II carbonate preparation device at the Serveis Científico-Técnicos from the University of Barcelona. Analytical precision was

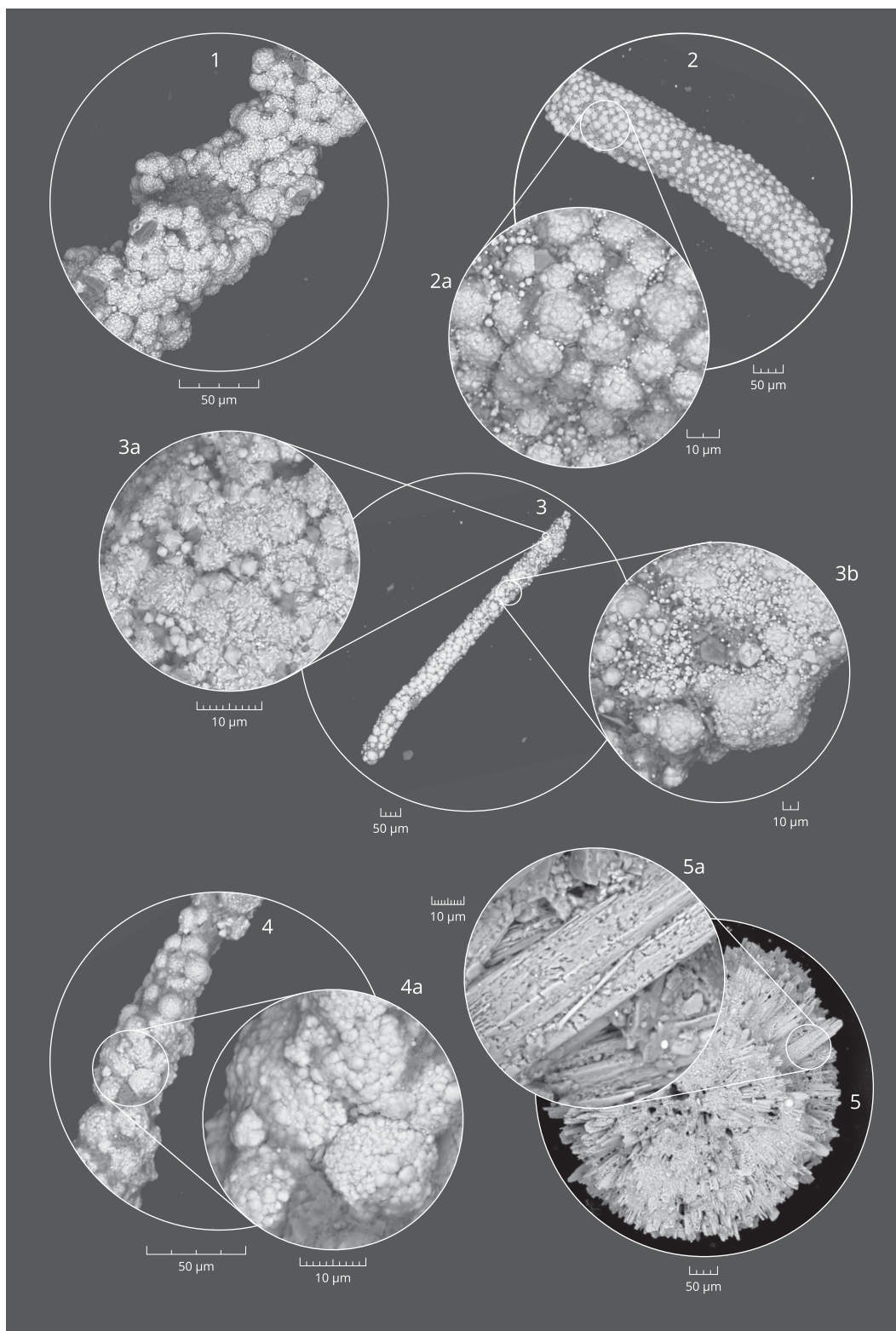


Figure 5. Scanning electron microscope images: (1)–(4) pyrite-encrusted tubes that precipitated in the methane-rich sediments during a very early stage of diagenesis (core GC09, from 260 cm, near the bottom of the section containing the investigated bivalves). (2a and 4a) Close-ups show famboidal pyrite. (3a and 3b) Close-ups of acicular aragonite crystals and 2 μm spheric crystals of pyrite. (5) Botryoidal aggregates of acicular aragonite crystals. (5a) Close-up of an acicular aragonite crystal formed on clay particles in section 457–498 of GC16.

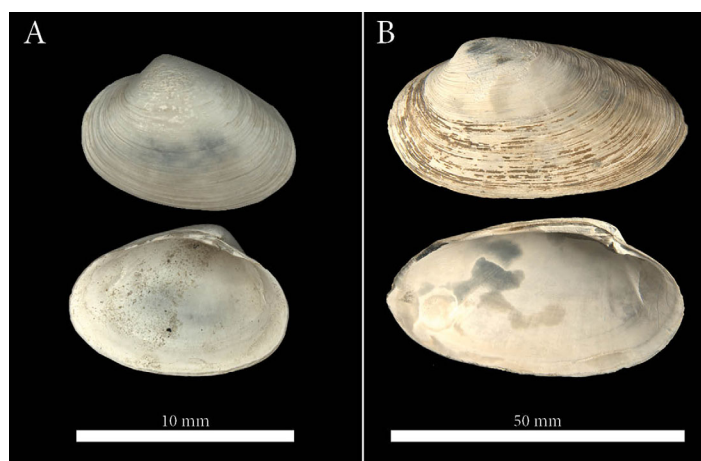


Figure 6. The two bivalve species that dominated the fossil bivalve community on the Vestnesa Ridge in both cores: (a) *Phreangena* s.l. and (b) *Isorropndon* sp.

GC16: 400–430 cm) that coincided with large anomalies in bulk density and, in the case of GC09, depletion in magnetic susceptibility (Figures 3 and 4). There was no evidence of bivalve shell material in other core sections of the two cores. We focused our sampling on these bivalve-rich core sections and on areas immediately above and below them. Large bivalve shells were removed from the bivalve-rich core sections prior to sectioning into ~1 cm thick samples.

In GC09, sediments from the entire core (300 cm in length) consist of dark gray clay and include shell components (Figure 3). A diatom-rich layer occurs in the top 10 cm of the core. In this core, the shell bed extends from approximately 236 to 268 cm and dry shell weight ranged from 0 to 0.083 g/cm³ of sediment (shell weight is presented per volume of sediment to correct for differences in volume among sediment sections), but shell material was not evenly distributed throughout the shell bed. Shell components account for up to ~40% of the material in the stratigraphic interval 236–268 cm with almost 90% of the total shell weight, corrected for sediment volume, concentrated in section 241–250 cm. At 250 cm, in the shell bed, we found a few specimens of the ostracod *Krithe huntii* with articulated valves. The specimens are juveniles with thin valves and a length of about 0.5 cm. The delicate valves can only be preserved in a stable environment and are indicative of *in situ* deposition of the sediment. The carbon and oxygen isotopic ratios of a carbonate nodule collected at 245 cm exhibited a $\delta^{13}\text{C}$ of -32.3‰ and $\delta^{18}\text{O}$ of 6.73‰ , respectively. Isolated polygenic litho-fragments reported as isolated clasts (<5 cm) were found in the intervals 20–100 and 230–265 cm (Figure 3). Calcium carbonate concretions (<1 cm) and pyrite-encrusted tubes (more than 63 μm in length and 0.20–0.50 μm in diameter) are also present in the upper 100 cm of the core and between 250 and 260 cm (Figure 5).

GC16 is 498 cm in length and is characterized by gray mud that varies from light to dark in specific intervals (Figure 4). The sediments had a strong odor of H₂S. Some intervals had black patches indicating organic matter enrichment. The shell bed extends from 400 to 430 cm and exhibits sharply defined upper and lower limits. Shell material accounts for ~50% of the sediment (dry weight) in the shell bed. The dry weight of shell material ranged from 0 to 0.095 g/cm³. The 421–426 cm section had the largest percentage of shell material (29.6% of total shell weight recovered), but there was significant shell material, including fragments of periostracum, as shallow as the 405–408 cm section. Below 426 cm, the amount of shell material diminished rapidly; we found only a few small fragments deeper than 430 cm. A carbonate nodule collected at 428 cm had a $\delta^{13}\text{C}$ of -30.7‰ and $\delta^{18}\text{O}$ of 4.92‰ . Isolated polygenic litho-fragments reported as clasts (<5 cm) occur between 190–210 and 340–380 cm. Micrite calcium carbonate concretions (<1 cm) exist in the lower part of the core between 470 and 498 cm. Laminated sediment occurs between 290 and 320 cm. A diatom-rich layer is prominent at 20–70 cm in the core; burrow-like pyrite concretions are rare. In the interval 457–498 cm, palisade and radiating structures contain acicular crystals of aragonite (Figure 5). In the interval 474–498, we found irregularly shaped nodules, up to 1 cm in diameter, reddish micrite and calcium carbonate concretions (Figure 5).

estimated to be better than 0.03‰ for $\delta^{13}\text{C}$ and 0.08‰ for $\delta^{18}\text{O}$ by measuring the certified standard NBS-19. Isotope results are reported in standard delta notation relative to Vienna Pee Dee Belemnite (V-PDB).

3. Results

3.1. Core Imaging and Lithology

The X-rays revealed abundant whole bivalve shells (including some large and small articulated individuals) and shell fragments in discrete sections of the cores (GC09: 236–268 cm;

Table 2. X-Ray Diffraction Determinations of % Aragonite and % Calcite in Shell Fragments of *Phreagena* s.l. and One *Isorropodon* sp. Whole Shell From Different Depth Intervals in Cores GC16 and GC09

Core	Depth Below Surface (cm)	Laboratory Code	Sample	Percent Aragonite (%)	Percent Calcite (%)
GC16	408–411	BCID-14658	<i>Phreagena</i>	100	0
GC16	417–421	BCID-14661	<i>Phreagena</i>	100	0
GC16	417–421	BCID-14662	<i>Phreagena</i>	100	0
GC16	417–421	BCID-14663	<i>Phreagena</i>	100	0
GC16	421–426	BCID-14664	<i>Phreagena</i>	90.3	9.7
GC16	421–426	BCID-14665	<i>Phreagena</i>	93	7
GC16	421–426	BCID-14666	<i>Phreagena</i>	91.8	8.2
GC09	242–250	BCID-14667	<i>Phreagena</i>	85.6	14.2
GC09	242–250	BCID-14667	<i>Phreagena</i>	100	0
Acetic Acid					
GC09	242–250	BCID-14668	<i>Phreagena</i>	100	0
GC09	242–250	BCID-14669	<i>Phreagena</i>	100	0
GC09	242–250	BCID-14670	<i>Phreagena</i>	93.4	6.6
GC09	242–250	BCID-14671	<i>Phreagena</i>	100	0
GC09	242–250	BCID-14745	<i>Isorropodon</i>	100	0

3.2. Shell Bed Bivalves and Foraminiferal Assemblages

Some of the bivalve shell material retrieved from shell beds in both of the cores were fragments, though there were several large and many smaller whole valves. A few valves were articulated indicating they likely died *in situ*. The individuals were identified as belonging to two genera of the bivalve family Vesicomidae: *Phreagena* s.l. and *Isorropodon* sp. (Figure 6). Most of the largest shell fragments that were selected for geochemical analysis belong to *Phreagena* s.l. We collected one whole (6 cm shell length) and one broken valve of *Phreagena* s.l. from GC09 from the 242–250 cm section and one large whole valve from the 243–246 cm section. There were also 14 whole *Isorropodon* sp. individuals (~1 cm shell length) from sections 241–243 cm (n = 2), 243–246 cm (n = 1), and 242–250 cm (n = 11). We collected large (5 cm shell length) whole and broken valves of *Phreagena* s.l. from GC16 from sections 408–411 cm (one whole valve and one broken), 411–414 cm (one whole), and 414–415 cm (one broken) as well as six whole *Isorropodon* sp. single and articulated shells (~1 cm shell length) from section 421–426 cm.

The benthic foraminifera assemblage in the shell bed interval of GC09 is consistently dominated by *Cassidulina neoteretis*, with less abundant *Melonis barleeaanum*, *Elphidium excavatum*, and *Stainforthia fusiformi*. In the upper part of the shell bed, *Sigmoilopsis schlumbergeri* occur rarely. Throughout the shell bed in GC16, the benthic foraminifera assemblage is consistently dominated by *Cassidulina neoteretis*, whereas *Elphidium excavatum* and *Stainforthia fusiformi* are less dominant. *Melonis barleeaanum* and *Miliolids* are rare. The planktonic assemblage in both GC09 and GC16 is dominated by *Noegloboquadrina pachyderma* (s) and *Turborotalita quinqueloba*. Accessory species are *Globigerina bulloides*, *Globigerinita glutinata*, and *Globigerinita uvula*. None of the identified species in the shell beds are endemic to the seep area and many of them are widespread in the Arctic Ocean [Bé and Tolderlund, 1971; Mackensen and Hald, 1988; Johannessen et al., 1994; Hald and Steinsund, 1996; Simstich et al., 2003; Jennings et al., 2004].

3.3. Stable Isotopes and ¹⁴C Dates

3.3.1. State of Preservation of Calcite Foraminifera and Bivalves

Planktonic foraminifera in both the GC09 and GC16 shell bed intervals exhibited a variable state of preservation, ranging from poor to moderate. We found evidence of dissolution and/or diagenetic alteration and broken specimens. Foraminifera tests are corroded and fragmented, with a secondary coating, and yellow to light brown color. Some foraminifera tests are recrystallized or have diagenetic calcite added (secondary overgrowth). The $\delta^{13}\text{C}$ of planktonic foraminifera ranged from -1.2‰ to -6.7‰ (Table 1).

Most the bivalve fragments or shells of *Phreagena* s.l. that were tested for carbonate composition using X-ray diffraction were 100% aragonite indicating no diagenesis or secondary deposition of calcite (Table 2). The few shell fragments that were not 100% aragonite contained between 6.6% and 14.4% calcite. The fragment treated with acetic acid had an initial composition of 14.4% calcite but was 100% aragonite after treatment. *Isorropodon* shells were very small and the entire shell was needed for XRD. Hence, we only analyzed one *Isorropodon* shell (GC09) and it was 100% aragonite (Table 2).

Table 3. $\delta^{13}\text{C}$ for Inorganic and Organic Shell Material From Both Species of Bivalves Collected at Selected Depth Intervals From Cores GC16 and GC09^a

Core	Depth Below Surface (cm)	Taxa	N (Inorganic/Organic)	Mean $\delta^{13}\text{C}$ Inorganic			Mean $\delta^{13}\text{C}$ Organic			Methane-Derived $\delta^{13}\text{C}$ (%)
				($\% \pm \text{SE}$)	Max ($\%$)	Min ($\%$)	($\% \pm \text{SE}$)	Max ($\%$)	Min ($\%$)	
GC16	408–411	<i>Phreagena</i>	3/3	0.91 ± 0.44	1.38	0.04	-23.14 ± 0.97	-21.33	-24.63	8.8–15.7
GC16	417–421	<i>Phreagena</i>	3/3	0.19 ± 0.94	2.36	-0.95	-22.93 ± 0.67	-21.6	-23.63	8.1–14.7
GC16	421–426	<i>Phreagena</i> ^b	2/3	0.08 ± 0.91	0.72	-0.56	-24.73 ± 0.79	-23.29	-26.00	13.1–23.6
GC16	421–426	<i>Isorropodon</i>	3/2	-5.63 ± 3.77	-0.64	-13.02	-26.79 ± 1.19	-25.6	-27.99	18.9–34.0
GC09	242–250	<i>Phreagena</i>	3/4	-3.69 ± 1.79	-2.16	-5.66	-25.45 ± 2.44	-22.72	-28.59	15.1–27.2
GC09	247–250	<i>Isorropodon</i>	5/4	-2.83 ± 0.68	-1.76	-5.46	-28.65 ± 0.43	-28.36	-29.28	24.0–43.2
Control	N/A	<i>Serripes</i> ^c	1/1	-1.33 ± 0.41			-19.76 ± 0.15	-18.51	-20.16	0

^aValues are number of replicates (N), mean (\pm standard error of the mean), maximum (max), and minimum (min). The last column presents the % $\delta^{13}\text{C}$ content of organic shell material that is attributed to methane-derived carbon. The ranges shown were derived from a two end member mixing model performed on the mean $\delta^{13}\text{C}$ values of individuals with methane end-member values of -56% (low values) and -40% (high values) and a modern control value of -19.8% .

^bTreated with acetic acid.

^cRepeated measurements from a single shell (4/10).

The $\delta^{13}\text{C}_{\text{inorganic}}$ values from individual *Phreagena* shells and shell fragments from both cores ranged from -5.66% to 2.36% (Table 3). The mean $\delta^{13}\text{C}_{\text{inorganic}}$ values for all depth intervals in GC16 were near 0% while the average value was -3.69% for the one depth interval in GC09.

Individual $\delta^{13}\text{C}_{\text{inorganic}}$ values from *Isorropodon* shells ranged from -13.02% to -0.64% (Table 3). The mean $\delta^{13}\text{C}_{\text{inorganic}}$ values for *Isorropodon* were negative in both GC09 and GC16; -2.83% and -5.63% , respectively. In GC09, *Isorropodon* and *Phreagena* shells had similar average values of $\delta^{13}\text{C}_{\text{inorganic}}$. In GC16, however, the mean $\delta^{13}\text{C}_{\text{inorganic}}$ of *Isorropodon* shells was -5.63% , considerably lighter than the values for *Phreagena* which as noted were near 0% .

The $\delta^{13}\text{C}_{\text{organic}}$ values in shells and shell fragments of both species were considerably lighter than the $\delta^{13}\text{C}_{\text{inorganic}}$ values (Table 3). The heaviest value for *Phreagena* was -21.33% from GC16 at the top of the shell bed. *Isorropodon* had lighter mean $\delta^{13}\text{C}_{\text{organic}}$ values than *Phreagena* in both cores and one replicate shell had a value as low as -29.28% .

The $\delta^{18}\text{O}$ from *Phreagena* ranged from 0.84% to 5.48% , over both cores, with most values greater than 3% (Table 4). Although replication is lacking in GC16, the obtained shell $\delta^{18}\text{O}$ values do not change with core depth. The mean $\delta^{18}\text{O}$ (3.60% , SE = 0.79) for shells from the one section in GC09 for which we have replication (242–250 cm) is not significantly different from the mean $\delta^{18}\text{O}$ (3.86% , SE = 0.37) from GC16 (one-way ANOVA, $p > 0.36$). Oxygen isotopes in seep clams often show considerable scatter, which may be due to temperature variations controlled by fluid-venting activity [Lietard and Pierre, 2008].

3.3.2. ^{14}C Dates

All the radiocarbon dates obtained for our bivalve shell material are reliable. The corrected ages for bivalves from GC16 are 17,543 years B.P. at a core depth of 414.5 cm and 17,707 years B.P. at 423.5 cm. In GC09, a bivalve sample from 237 cm indicates an age of 16,680 years B.P.

Table 4. $\delta^{13}\text{C}$ and $\delta^{18}\text{O}$ for Shell Material From *Phreagena* s.l. (Fragments or Parts of Whole Shells) Collected at Selected Depth Intervals From Cores GC16 and GC09

Core	Depth Below Surface (cm)	Laboratory Code	$\delta^{13}\text{C}$ ($\%$)	$\delta^{18}\text{O}$ ($\%$)
GC16	408–411	BCID-14658	3.44	3.63
GC16	411–414	BCID-14728	3.24	4.45
GC16	414–415	BCID-14279	2.41	4.71
GC16	417–421	BCID-14661	1.13	4.18
GC16	417–421	BCID-14662	3.12	4.34
GC16	417–421	BCID-14663	1.64	1.99
GC16	417–421	BCID-14725	1.94	3.15
GC16	421–426	BCID-14726	-1.57	4.44
GC09	242–250	BCID-14733	1.32	5.48
GC09	242–250	BCID-14667	1.26	0.84
GC09	242–250	BCID-14668	-3.03	3.29
GC09	242–250	BCID-14669	-0.11	3.58
GC09	242–250	BCID-14671	1.21	4.84
GC09	243–246	BCID-14764	-0.09	5.33

Although we selected well-preserved specimens of the planktonic foraminifera *N. pachyderma*, we rejected the ages we obtained because the samples displayed anomalous $\delta^{13}\text{C}$ values (-3.10 and -3.7‰ in core GC16 and from -5.10 to -6.7‰ in GC09) (Table 1). The normal $\delta^{13}\text{C}$ range of *N. pachyderma* (s) in the same region is between approximately -0.5‰ and 1‰ [Volkman and Mensch, 2001; Nørgaard-Pedersen et al., 2003; Sarnthein et al., 2003; Jessen et al., 2010]. In general, planktonic foraminifera cannot record the signal from methane in the water column since most of the methane that has escaped from the seafloor is likely consumed by methanotrophic bacteria in both the sediment and water column [Dickens, 2001; Reeburgh, 2007; Consolaro et al., 2015]. Therefore, we attribute the negative values to secondary precipitation of methane-derived authigenic carbonate on the foraminiferal shells after deposition on the seafloor [Torres et al., 2003, 2010; Millo et al., 2005; Panieri et al., 2009]. These lighter carbon isotope values of planktonic foraminifera can shift the obtained sample ages toward older values [Gulin et al., 2003; Panieri et al., 2014]. Accordingly, we rejected the ages obtained for our *N. pachyderma* samples with depleted $\delta^{13}\text{C}$. The ages of two samples, however, were considered reliable. Below the shell bed, at a core depth of 460.5 cm (GC16), the corrected age from dated planktonic foraminifera (with acceptable $\delta^{13}\text{C}$) is 24,743 B.P. In GC09, a planktonic foraminifera sample (also with acceptable $\delta^{13}\text{C}$) close to the top of the shell bed yielded a date of 21,031 years B.P.

4. Discussion

To our knowledge, this is the first discovery of ancient chemosynthesis-based bivalve communities in the high Arctic. We use four lines of evidence to suggest that the discovered shell beds are linked to a paleo-seepage event lasting ~ 1000 years at Vestnesa Ridge: (1) the predominance of bivalve species known to be associated with oceanic vents and seeps; (2) $\delta^{13}\text{C}_{\text{inorganic}}$ (shells and planktonic foraminifera); (3) shell $\delta^{13}\text{C}_{\text{organic}}$ values indicating carbon derived from methane; (4) the presence of methane-derived authigenic carbonates. In addition, the presence of pyrite-encrusted fossil worm tubes is consistent with the scenario we propose. By integrating our shell bed chronology into a regional chronological framework, we are further able to shed new light on the timing and mechanisms that can trigger such seepage events.

4.1. Shell Beds Are Linked to a Past Major Seepage Event

4.1.1. Chemosynthesis-Based Bivalve Communities

Dense collections of bivalves and bivalve fragments are prominent features in X-rays of the two gravity cores from Vestnesa Ridge. Bivalves are only present in large numbers in discrete depth intervals in our cores: 236–268 cm in GC09 and 400–430 cm in GC16. The sediment in the shell bed is similar to the sediment in the remainder of the cores, excluding the possibility that the shells were eroded and transported. In addition, the base of the shell bed is not erosive. The two dominant bivalve species that make up most of the material in the discrete horizons of bivalve shells (*Phreagena* s.l. and *Isorropodon* sp.) belong to the family Vesicomidae. The Vesicomidae are widely distributed at hydrothermal vents and hydrocarbon seeps where they can reach very high densities [Krylova and Sahling, 2010; Taylor and Glover, 2010], and are sustained by H_2S . Both species belong to the newly recognized subfamily Pliocardiinae, all members of which rely on sulfide-reducing endosymbiotic bacteria for nutrition [Krylova and Sahling, 2010]. *Phreagena* is known from the eastern and western Pacific and northern Indian Oceans [Krylova and Sahling, 2006, 2010], a panthalassic range, where it is associated with vents and seeps. The only other record of *Phreagena* in the Atlantic is from near the Rainbow Hydrothermal vent field on the Mid-Atlantic Ridge ($36^{\circ}13' \text{N}$) where large numbers of fossil shells are present [Lartaud et al., 2010]. *Isorropodon* is widely distributed at vents and seeps in the Atlantic and Pacific oceans along continental margins [Lartaud et al., 2010]. Until now, the most northern record of the genus in the Atlantic is a newly described species from a methane seep on the Norwegian continental margin at approximately 64°N [Krylova et al., 2011; Krylova and Sahling, 2010].

The high concentrations of these two species of bivalves in both of our cores represent the first evidence of bivalve-dominated seep communities in the Arctic, while the spatial variation in the abundance of bivalve shells and fragments in these cores suggests that the methane emissions supporting the bivalve community varied considerably through time and space. It is the first time that chemosynthetic bivalve communities have been documented as far north as 79°N .

Table 5. $\delta^{13}\text{C}$ for Modern and Fossil Vesicomidae From Methane Seeps and Hydrothermal Vents (n.d. = No Data; n.a. = Not Applicable)^a

Taxon	Habitat	Mean $\delta^{13}\text{C}$ Inorganic (\pm SE)	Max	Min	Reference
<i>Vesicomidae</i> sp. (fossil)	Seep	-16.4 ± 1.2	-12.9	-18.9	Hein et al. [2006]
<i>Calyptogena</i> sp. (fossil)	Seep	-3.3	n.a.	n.a.	Mae et al. [2007]
<i>Calyptogena soyoae</i>	Seep	-2.3	n.a.	n.a.	Mae et al. [2007]
<i>Calyptogena solidissima</i>	Seep	4.2	n.a.	n.a.	Mae et al. [2007]
<i>Calyptogena</i> sp.	Mud volcano	n.d.	0.3	-0.2	Lietard and Pierre [2009]
<i>Calyptogena</i> sp.	Trough	n.d.	0.8	-0.6	Lietard and Pierre [2009]
<i>Calyptogena</i> sp.	Seep	n.d.	1.2	0.7	Lietard and Pierre [2009]
<i>Vesicomya</i> sp.	Brine pool	n.d.	3.0	-7.3	Lietard and Pierre [2009]
<i>Calyptogena magnifica</i>	Vent	n.d.	3.7	1.9	Lietard and Pierre [2009]
<i>Phreagena</i> sp. (fossil)	Vent	5.16 ± 0.62	8.35	2.86	Lartaud et al. [2010]
<i>Calyptogena</i> sp. (fossil)	Seep	2.3 ± 0.35	2.7	2.1	Han et al. [2014]
<i>Phreagena</i> sp. (fossil)	Seep	-0.77 ± 0.64	2.36	-5.66	This Study
<i>Isorropodon</i> sp. (fossil)	Seep	-2.83 ± 0.68	-0.64	-13.0	This Study

^aBold data are from this paper.

4.1.2. Inorganic Carbon Isotope ratios

The inorganic carbon isotope ratio in bivalve shells is derived predominantly from dissolved inorganic carbon (DIC). The ratio may be influenced by metabolism; for taxa with symbiotic bacteria, it is also influenced by the metabolic pathway. Hence, the carbon isotopic signatures of shell inorganic carbon reflect ambient conditions to varying degrees [McConnaughey et al., 1997; McConnaughey and Gillikin, 2008; Owen et al., 2008; Lartaud et al., 2010; Butler et al., 2011; Nedoncelle et al., 2014]. Hein et al. [2006] suggested that extremely depleted $\delta^{13}\text{C}_{\text{inorganic}}$ in shells is indicative of a reducing environment, but the range of values in shells from seeps reviewed by Lietard and Pierre [2009] showed -10‰ to $+3.5\text{‰}$, and from just the Vesicomidae from -16.4‰ to $+5.2\text{‰}$ (Table 5). Extremely light $\delta^{13}\text{C}_{\text{inorganic}}$ values suggest that a large portion of the HCO_3^- being used to construct carbonate is derived from Anaerobic Oxidation of Methane (AOM) [Hein et al., 2006] or from sulfate reduction, but values as heavy as $+5.6\text{‰}$ are also recorded from some taxa associated with vents or seeps. It is important to note that the lightest $\delta^{13}\text{C}_{\text{inorganic}}$ value for Vesicomidae (-16.4‰) [Hein et al., 2006] may have been compromised by diagenesis [Paull et al., 2008].

The values we measured for both species are within the range of values recorded from other vent and seep sites (Table 5). Excluding the Hein et al. [2006] data point, the $\delta^{13}\text{C}_{\text{inorganic}}$ values recorded in seep bivalves are not as depleted as one might expect for bivalves living in a reducing environment. The Vesicomida, however, use near-bottom water taken in through their siphons as one source of bicarbonate for shell construction and they live only partially burrowed in the sediment [Taylor and Glover, 2010]. Nevertheless, most of the mean $\delta^{13}\text{C}_{\text{inorganic}}$ measurements of core bivalves are lighter than the nonseep bivalve *Serripes gronelandicus* we used for comparison (Tables 3 and 5).

Methane emissions might have varied over the period of the communities' existence at each site, but slight differences in shell chemistry between, as well as within, sites could be explained by differences in individual distributions relative to the source of methane. Therefore, these differences cannot be easily used to distinguish between amplitudes of methane flow. Finally, the metabolic pathways, whether the symbionts are methanotrophic, thiotrophic, or a combination of the two can influence the isotopic fractionation of the carbon in shells [Nedoncelle et al., 2014]. The negative $\delta^{13}\text{C}$ values recorded in planktonic foraminifera (-6.7‰ to -3.1‰ ; Table 1) as a result of postdepositional diagenesis further confirms the presence of significant amounts of methane in the environment. Using only shell $\delta^{13}\text{C}_{\text{inorganic}}$ values as an indication of methane-derived carbon could be misleading if shells underwent diagenesis, as suggested by Paull et al. [2008], or if authigenic calcite derived from methane was deposited on their shell surfaces. In fact, light $\delta^{13}\text{C}_{\text{inorganic}}$ values from seeps might also be a consequence of secondary deposition of carbonates with methane-derived carbon. We found limited evidence; however, that diagenesis occurred in the bivalves, which suggests that the $\delta^{13}\text{C}_{\text{inorganic}}$ values we recorded are not artifacts.

4.1.3. Organic Carbon Isotope Ratios

Shell organic material reflects an animal's food source [O'Donnell et al., 2003; Mae et al., 2007; Carmichael et al., 2008] and the $\delta^{13}\text{C}_{\text{organic}}$ can be used to differentiate between possible sources of nutrition in marine habitats including at vents and seeps. In seep communities that are dominated by several isotopically

distinct carbon sources (e.g., methane, phytoplankton-derived detritus, terrestrial vegetation, and organic carbon synthesized by chemoautotrophs), carbon isotope analysis provides a robust tracer of carbon sources at the base of the food web [Levin and Michener, 2002; Thurber et al., 2010]. Methane is especially easy to document in food chains because it is strongly depleted in ^{13}C ($\delta^{13}\text{C} -75\text{‰}$ to -28‰) compared to other sources [Van Dover, 2007]. Macroinfauna at seeps typically have tissue $\delta^{13}\text{C}$ values lighter than approximately -24‰ indicating at least some dependency on methane-derived carbon [Levin, 2005]. $\delta^{13}\text{C}_{\text{organic}}$ values in our shells of *Phreagena* and *Isorropodon* ranged from -21.33‰ to as light as -29.28‰ (Table 3). These values were 4–10‰ lighter than those from the modern control suspension-feeding *Serrripes groenlandicus*, indicating a contribution from methane-derived carbon to the seep clams' nutrition and reflecting the chemosynthetic endosymbionts on which these clams at least partially depend.

In order to assess this contribution, we perform a two-end member mixing model using the six individual $\delta^{13}\text{C}_{\text{organic}}$ values of the shell organic material (Table 3):

$$X = z^*(Y) + (1 - z)^*C, \quad (1)$$

with variables defined as follows:

$C = \delta^{13}\text{C}_{\text{organic}}$ contribution from phytoplankton-derived carbon (modern control value),
 $X = \delta^{13}\text{C}_{\text{organic}}$ measurements in shell material (sample mean value),
 $Y = \delta^{13}\text{C}_{\text{organic}}$ contribution from methane-derived carbon (methane end-member value),
 $z =$ fraction of methane-derived $\delta^{13}\text{C}_{\text{organic}}$ content.

A range of $\delta^{13}\text{C}$ values for methane have been recorded on the continental margin west of Svalbard. Sahling et al. [2014] measured -55.7‰ from shallow water on the shelf and Fisher et al. [2011] recorded -45.7‰ from a 1210 m deep pockmark on Vestnesa Ridge. We derived a range of values for each individual bivalve sample by using methane end-member values of -56‰ and -40‰ , allowing for partial preferential oxidation of light carbon in methane in the sediments by methanogens [Fisher et al., 2011] and reflecting the heavier end of a range of measured values of $\delta^{13}\text{C}$ of DIC in the water of methane seeps [Aharon et al., 1992]. Solving equation (1) for "z" and multiplying by 100, the estimated contribution to $\delta^{13}\text{C}_{\text{organic}}$ from methane-derived carbon ranges from 8% to 43%. Based on the $\delta^{13}\text{C}_{\text{organic}}$ values we recorded, and considering the good state of preservation of the shell organic material, it is clear that our two species of Vesicomidae are relying to varying degrees on endosymbionts, similar to other members of this taxonomic group. These results, the first as far as we know from a seep bivalve, also indicate that these taxa obtain the majority of their nutrition from photosynthetically derived material.

The only other study that has measured the carbon isotopic signature in the organic component of Vesicomidae (*Calyptogena*) shells recorded values of -34.6‰ to -32.3‰ for modern individuals from a vent and -28.5‰ for Vesicomidae fossils from the Pliocene [Mae et al., 2007]. As was the case with the $\delta^{13}\text{C}_{\text{inorganic}}$ from our samples, the $\delta^{13}\text{C}_{\text{organic}}$ in the individuals from core GC09 was lighter by 2–3‰ compared to individuals from core GC16 (Table 3). Differences in $\delta^{13}\text{C}$ values among vents have been attributed to differences in "seepage activity" [Levin, 2005], but again might also be due to small-scale differences in distribution relative to methane seepage or different metabolic pathways of their endosymbionts.

4.1.4. Methane-Derived Authigenic Carbonates

Carbonate precipitation is a striking phenomenon that occurs at seeps as a result of coupled bacterial sulfate reduction and methane oxidation [Ritger et al., 1987; Paull et al., 1989; Peckmann et al., 1999]. This reaction is associated with an increase in alkalinity which favors carbonate precipitation. It is widely accepted that methane-derived carbonates preferentially form within the sediment [Paull et al., 1989; Gaillard et al., 1992; Thiel et al., 1999]. Field and laboratory studies indicate that methane is oxidized by a consortium of archaea and sulfate reducers [Hoehler et al., 1994; Boetius et al., 2000; Treude et al., 2003]. Marine bottom waters are usually oxic, so carbonate formation induced by anaerobic oxidation of methane will be confined to anoxic sediments. In our core, carbonate concretions with depleted values clearly indicative of precipitation in the presence of AOM ($\delta^{13}\text{C}$ is -32.3‰ in GC09 and -30.7‰ in GC16) suggest that fluid continued to seep after the bivalve community was extinct because these species of bivalves live at the sediment surface and the bottom water would have been well oxygenated. This also explains the negative $\delta^{13}\text{C}$ signal from our planktonic foraminifera due to the formation of methane-derived authigenic carbonates on the foraminifera shell.

In methane seep environments, aragonite is frequently the main authigenic carbonate to be represented in shallow crusts and concretions related to AOM [e.g., *Bohrmann et al.*, 1998; *Peckmann et al.*, 2001; *Pierre et al.*, 2012]. Aragonite precipitation is favored over calcite in conjunction with high rates of AOM sustained by vigorous methane fluxes, which results in oversaturation with respect to bicarbonate at relatively high pore water sulfate concentrations near the seafloor [*Greinert et al.*, 2001; *Peckmann et al.*, 2001; *Aloisi et al.*, 2002; *Luff and Wallmann*, 2003]. We observed acicular crystals of aragonite in GC16 core interval 457–498 cm (Figure 5). Aragonite crystals occurred at the base of the shell bed in GC16 suggesting that they precipitated near the seafloor under conditions of intense fluid seepage activity. This intense fluid flow probably created the conditions for the establishment of the bivalve community.

In core GC09, abundant burrow-like pyrite concretions occur at the base of the shell bed. The identification of the (pyrite-encrusted tubes) fossil pyrite tubes as polychaetes is tentative; however, the similarity in the width of modern polychaete tubes (0.24–0.42 mm) collected from living polychaetes associated with nearby seeps and the fossil pyrite tubes suggests that the pyrite tubes belonged to polychaetes. Energy dispersive spectroscopy revealed that concretions on the tubes were composed of largely iron and sulfur with lesser amounts of silica, confirming that the encrusting material was pyrite.

These four lines of evidence support our hypothesis that these ancient shell beds are linked to a past seepage event at Vestnesa Ridge.

4.2. Shell Beds Constrain the Duration of a Past Seepage Event

We develop a regional chronological framework in order to interpret the processes leading up to the onset of the methane seep event and the establishment of the shell beds in our two gravity cores. This framework combines the stratigraphic information we obtained from our two cores with information obtained from previous investigations in the same region (Figure 7). Specifically, we combine our shell bed information with three well-described stratigraphic intervals [*Elverhøi et al.*, 1995; *Rasmussen et al.*, 2007; *Jessen et al.*, 2010; *Consolaro et al.*, 2015].

1. Diatom-rich layer: there is a diatom-rich layer in both our cores at the top 10 cm in GC09 and between 20 and 70 cm in GC16 (Figure 7). This represents the early Holocene diatom maximum originally observed in Fram Strait by *Stabell* [1986] and attributed to the northward movement of the Polar Front [*Jansen et al.*, 1983; *Stabell*, 1986]. In contrast to the Last Glacial Maximum (LGM), the warm Atlantic water incursion in the area at the beginning of the Holocene favored a peak in diatom productivity [*Koç et al.*, 1993]. *Jessen et al.* [2010] dated the diatom-rich layer between $10,100 \pm 150$ and 9840 ± 200 cal years (calendar years) B.P. This implies that the top of core GC09, representing approximately 10,000 cal years B.P., is missing.
2. Laminated deposits: we believe the laminated deposit at depth interval 290–320 cm in GC16 corresponds to the laminated layer previously described and dated to around 14,000 cal years B.P. from other sites in the area: $14,700 \pm 225$ to $14,380 \pm 220$ cal years B.P. [*Jessen et al.*, 2010]; $14,480 \pm 160$ to $14,000 \pm 65$ cal years B.P. [*Nørgaard-Pedersen et al.*, 2003; *Birgel and Hass*, 2004]; $14,290 \pm 140$ to 3950 ± 75 cal years B.P. [*Peersen*, 2006]. This probably corresponds to the early Bølling interstadial. *Jessen et al.* [2010] suggested that the widespread layer could be the result of one widespread Arctic meltwater event and for this reason its occurrence in sediment is near synchronous from the slope of the Yermak plateau to the Storfjorden Fan and throughout the Fram Strait. In GC09, a fine-grained homogeneous sediment section between 172 and 210 cm is considered to be the laminated section (Figure 3). The delicate laminae were likely destroyed when freezing the core. The fine-grained homogeneous sediment section is directly underlain by a layer rich in isolated clasts (<5 cm) at a core depth of 210–230 cm. This sediment section underlying the diatom-rich layer has also been identified in *Jessen et al.* [2010] and dated to $15,160 \pm 145$ to $14,700 \pm 225$ cal years B.P.
3. Clast-rich interval: in GC16, the laminated meltwater deposits described above are underlain by a clast-rich interval between 345 and 380 cm. We believe this layer is consistent with the clast-rich layer mentioned and dated by *Jessen et al.* [2010], and thus we also use it as a marker horizon along with the diatom-rich and laminated interval.

The shell bed in core GC16 covers about 30 cm (from 430 to 400 cm). The dates we obtained were from shells at core depths of 423 cm (17,707 years B.P.) and at 414 cm (17,543 years B.P.). We cannot use these

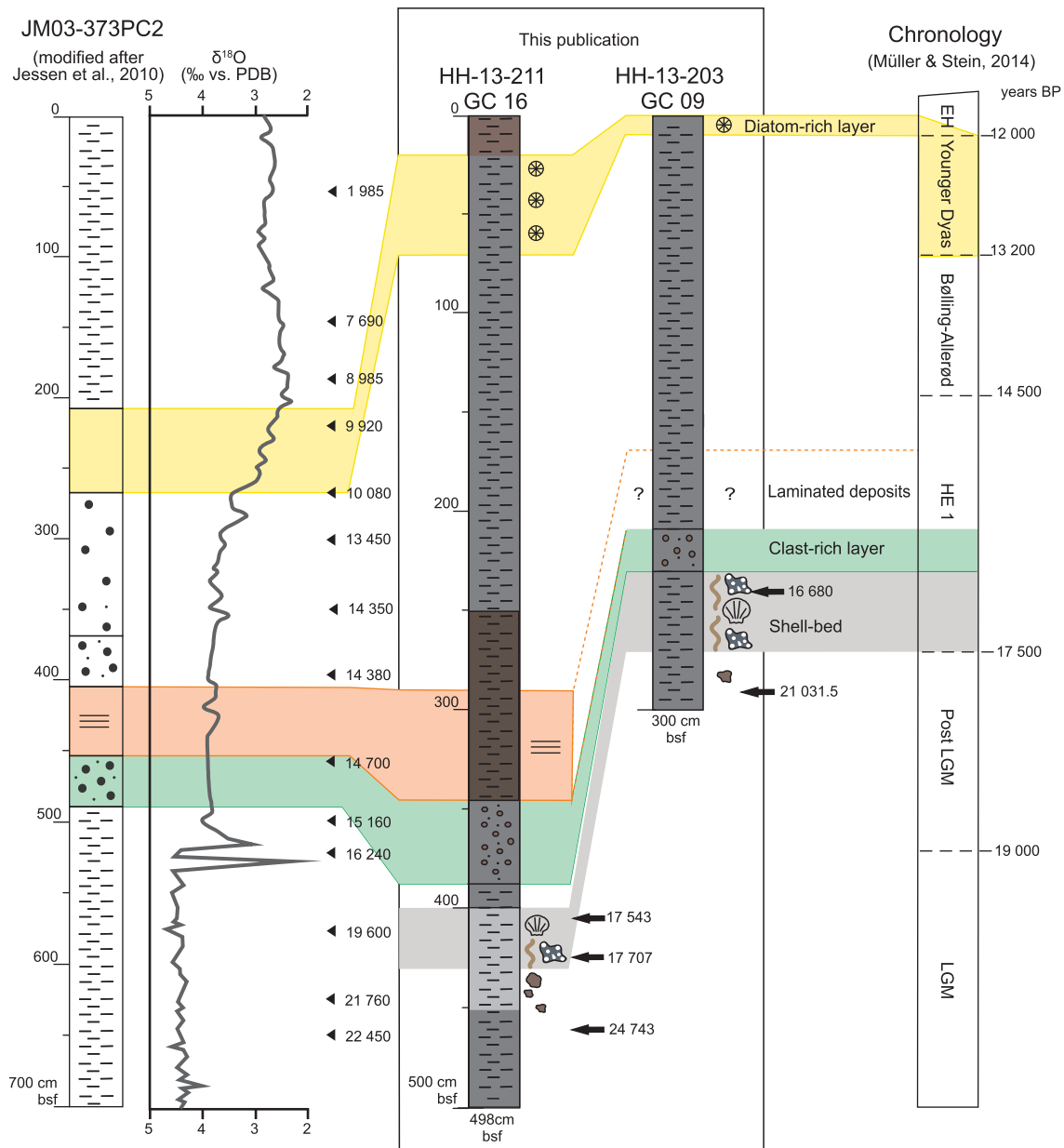


Figure 7. Chronological framework of the cores GC16 and GC09 (center) in relation to the lithological description of core JM03-373PC2 (leftmost), radiocarbon dates of stratigraphic key intervals, and $\delta^{18}\text{O}$ values given in *Jessen et al. [2010]* from the southwestern Svalbard margin (Storfjorden Trough Mouth Fan). Radiocarbon dates (^{14}C kyr B.P.) are indicated by black triangles for $\delta^{13}\text{C}$ values inside the range of normal marine values. The geological time scale (rightmost) is adopted from *Müller and Stein [2014]*. The dashed lines indicate a chronological boundary. EH—Early Holocene, HE 1—Heinrich Event 1, and LGM—Last Glacial Maximum. See Figure 4 for legend.

dates to estimate a sedimentation rate because the shells occupy a significant volume of the total sediment, leading to an unrealistically high sedimentation rate. By using the sedimentation rate obtained by *Consolaro et al. [2015]* and *Panieri et al. [2014]* of ~ 0.18 cm/yr and the ages at the base and the top of the shell bed, we estimate the duration of the living bivalve community to be approximately 1000 years. Furthermore, considering that the two dates from GC16 are from the base and middle of the shell bed, while the date from GC09 is from the top of the shell bed, we postulate that the shell beds in these two cores coevolved over the time period of 17,707–16,680 years B.P.

This chronology agrees with the relatively low IRD (Ice Rafted Debris) concentration and sedimentation rates from circa 20,000 to 15,600 cal years observed by *Jessen et al. [2010]* in the same area. The regional

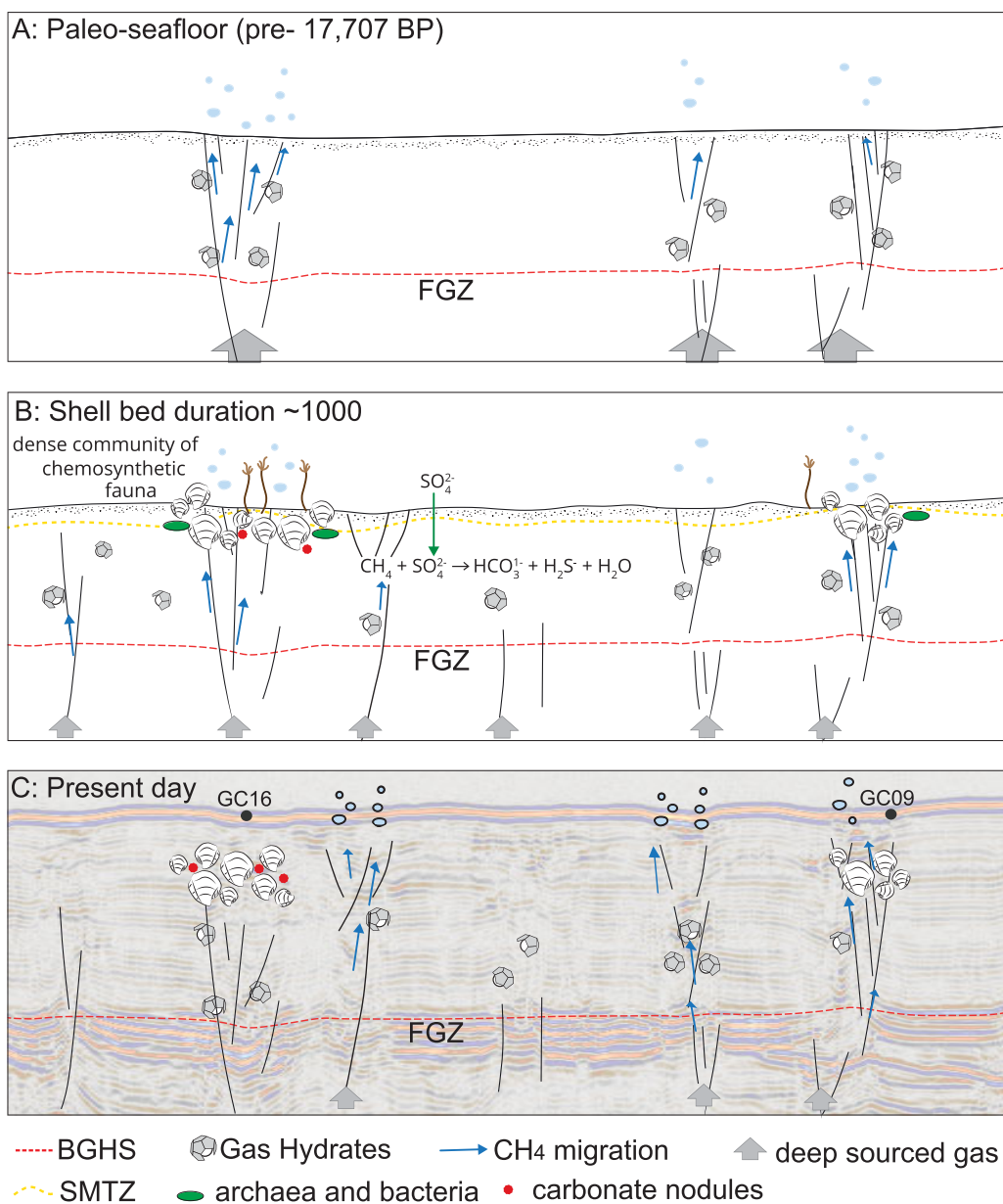


Figure 8. Model of seeps and bivalve community development. BGHS = base of the gas hydrate stability zone; FGZ = free gas zone; SMTZ = sulfate-methane transition zone. (A) Paleo-seafloor before the establishment of the chemosynthetic community with archaea and bacteria, Vesicomidae, and tube worms. (B) A period of ~1000 years of methane seepage that sustained the chemosynthetic communities. Precipitation of authigenic calcium carbonate occurs at the SMTZ that can outcrop on the seafloor and also control the spatial distribution of chemosynthetic communities. In our cores, authigenic carbonate concretions are restricted to the shell bed in GC16. (C) Present-day observations superimposed on high-resolution seismic data. Shell beds are buried; methane seepage occurs at some of the previously active gas chimneys (e.g., site GC09) while some of the chimneys appear dormant (e.g., site GC16). Gas hydrates are generally stable and seepage is most likely sustained by fluid migration from the FGZ through fractures into the hydrate zone with eventual release at the seafloor.

chronology framework provides a temporal context within which to evaluate the postulated controls and mechanisms connected to methane seepage events at deep water hydrate deposits [Plaza-Faverola et al., 2015; Hustoft et al., 2009]. These mechanisms have yet to be fully elucidated.

4.3. Potential Triggers of Seepage at Seafloor Pockmarks

Seafloor pockmarks along Vetsnes Ridge, some of them relict and some actively seeping gas (Figure 2), are associated with fluid expulsion through vertical conduits known as gas chimneys [e.g., Bünz et al., 2012]. Gas

hydrates have been perennially stable on Vestnesa Ridge for millions of years [Johnson *et al.*, 2015], implying the presence of hydrates as well as free gas trapped beneath hydrate bearing sediments (Figures 2a and 8c). The presence of buried pockmarks at specific stratigraphic intervals within gas chimneys is believed to indicate that seepage is an episodic process. These features have been observed at several continental margins, e.g., the Gulf of Lion, the mid-Norwegian margin, the Hikurangi margin, and the Congo Basin [Andresen and Huuse, 2011; Davy *et al.*, 2010; Plaza-Faverola *et al.*, 2015, 2011; Riboulot *et al.*, 2014]. Along Vestnesa Ridge, detailed 3-D seismic imaging of chimney structures show the presence of buried stacks of pockmarks intercalated with periods of undisturbed, well-stratified layers which based on stratigraphic constraints [Mattingsdal *et al.*, 2014], has been correlated with the onset and intensification of glaciations starting 2.7 Ma ago [Plaza-Faverola *et al.*, 2015]. In addition, the same study documents the link between the distributions of gas chimneys and faults (Figure 2) and suggests the occurrence of shorter-term seepage events modulated by faulting in the region [Plaza-Faverola *et al.*, 2015]. Using the age control dates acquired from the shell beds, and assuming that they indicate methane seepage, we can ask: What does the timing and duration of this past methane seepage event reveal about the physical processes controlling methane seepage along Vestnesa Ridge?

Here we focus on two time periods: post Last Glacial Maximum (LGM) and Holocene. In this part of the stratigraphic record ~23,000 years, multiple methane emission events have been identified using carbon isotopic signatures of foraminifera from gravity cores collected from Vestnesa Ridge [Panieri *et al.*, 2014; Consolaro *et al.*, 2015]. At about 17,600 years B.P., which corresponds approximately to the appearance of shell beds, sea ice-free summers returned to the continental shelf region [Müller and Stein, 2014]. IP25 concentrations, an indicator of sea ice conditions, declined abruptly along the western continental margin of Svalbard accompanied by a drop in sea-ice biomarkers in a core from the same area [Müller and Stein, 2014]. Rising Mg/Ca temperatures [Benway *et al.*, 2010] and decreasing planktonic $\delta^{18}\text{O}$ values in the North Atlantic [Grousset *et al.*, 2001; Dokken and Jansen, 1999] support this interpretation. Taken together, the evidence indicates that the seepage event identified from the bivalve shell beds (17,707–16,680 B.P.) was post LGM.

Rising sea level and increasing bottom water temperatures following the LGM are two competing mechanisms (i.e., the hydrate stability field increases with rising pressures and decreases with rising bottom water temperatures [Sloan and Koh, 2008; Dickens and Quinby-Hunt, 1994]) that are expected to have affected the thickness of the GHSZ across the west-Svalbard margin. How significant the effects of climate-related pressure and temperature changes have been on hydrate systems across the margin is dependent on their distance from the shelf break (i.e., water depths). At the water depth of Vestnesa Ridge (>1000 m), bottom water temperatures at the time of the growing bivalve shell beds (~17,000 B.P.) changed only slightly with respect to the permanently cold temperatures observed at present [e.g., Rasmussen *et al.*, 2007]. A temperature increase of several degrees would have been necessary to cause a significant decrease in the GHSZ thickness and hydrate dissociation at such water depths (pressures); while a progressive pressure increase due to a rising sea level during deglaciation would have favored hydrate stability [e.g., Dickens and Quinby-Hunt, 1994]. A model of hydrate dissociation by significant fluctuations in the thickness of the GHSZ in response to climatic changes would thus not be suitable to explain the 1000 years seepage event identified by the bivalve layers at Vestnesa Ridge. Additional mechanisms have to be evoked.

Recently, Plaza-Faverola *et al.* [2015] investigated fine-scale (<10 m broad) subseabed faults and fractures associated with the distribution of gas chimneys along Vestnesa Ridge (Figure 2c). These authors postulate that the imaged faults are an expression of shear deformation and that tectonic stress distribution and fault activity may have been a major mechanism controlling gas chimney formation and seepage. Active faults increase permeability and the associated fracture networks, in this case leading to gas chimney formation, favor focused fluid flow and seepage [Roberts *et al.*, 1996]. Fluid expulsion through faults and fractures can be a cyclic mechanism where pore fluid pressure builds up, followed by a peak of seepage and subsequent pressure drop. The duration of a single cycle will be dependent on the permeability of the fractures and the pressure buildup. It can vary from a few to thousands of years [e.g., Roberts and Nunn, 1995; Roberts *et al.*, 1996; Sibson, 1996]. The 1000 year time interval seepage event identified by the bivalve layers at Vestnesa Ridge fits the above model. If the seepage event indicated by the bivalve layers is assumed to be triggered by fault reactivation, then the time span the layer represents (i.e., 1000 years) is an approximation of an overpressure pulse leading to the release of free gas trapped beneath hydrate bearing layers (Figure 2a) through gas chimneys already developed along the fault planes (Figure 8c). This scenario accounts for small-scale hydrate

dissociation caused by the contact of advecting warm fluids through faults and fractures into the hydrate system [Hornbach *et al.*, 2012] as an additional mechanism partially sustaining seepage (Figure 8).

To summarize, we argue that a fault reactivation episode may explain the seepage event inferred by the bivalve layers restricted to fault-related gas chimneys along Vestnesa Ridge. Fault movements at Vestnesa Ridge can be controlled by seismological activity in response to tectonic stress [Plaza-Faverola *et al.*, 2015] or by the added effect of tectonic stress and ice sheet flexural rebound forces [e.g., Stewart *et al.*, 2000].

5. Conclusions

Ours is the first report of chemosynthesis-based bivalve communities in the high Arctic. Dense shell beds with abundant and complete in situ shells, as well as bivalve fragments of the family Vesicomidae, reveal seabed paleo-communities associated with two pockmarks. The seep environment is characterized by depleted $\delta^{13}\text{C}$ values for both inorganic and organic shell material, methane-derived authigenic carbonates with depleted $\delta^{13}\text{C}$, and depleted $\delta^{13}\text{C}$ values for planktonic foraminifera. Shell beds are associated with sustained methane seepage during the last deglaciation about 17,500 years B.P. The patchy distribution of mineralogies (e.g., carbonate nodules, pyrite, aragonite) related to methane seepage suggests temporal changes in the magnitude of flow and in seep fluid chemistry as a result of localized percolation of methane-enriched pore fluids.

We estimate that the community persisted for approximately 1000 years, though the flux of methane may have varied over that time period leading to changes in faunal abundances. The persistence of shell beds for circa 1000 years can correspond to fluid expulsion associated with episodes of faulting and fracturing. The patchy spatial distribution of the shell beds indicates that fluid flow was channelized through gas chimneys along subseabed faults. This implies that these methane seeps and their associated communities should be limited in area and highly concentrated.

Regardless of the mechanism(s) causing the onset of methane seeping, bivalves (and likely other soft-bodied chemosynthetic-dependent taxa that would not be preserved) colonized seeps on the Vestnesa Ridge about 17,700 years B.P. By approximately 16,680 years B.P., seepage along faults was either insufficient to support the bivalve community or other undetermined factors caused the community's demise.

Acknowledgments

The Norwegian Research Council funded this research through the CAGE-Center for Arctic Gas Hydrate, Environment and Climate (grant 223259). We are indebted to E. M. Krylova (Laboratory of Ocean Benthic Fauna, P. P. Shirshov Institute of Oceanology, Russian Academy of Sciences) for identifying the bivalves and Joel Johnson for collecting the cores. We thank the crew of R/V Helmer Hanssen. Jürgen Mienert, Joanne Muratori, Michael Retelle, Marta Torres, and two anonymous reviewers provided valuable comments on earlier versions of this manuscript. W. G. Ambrose received partial sabbatical support from Bates College. W. G. Ambrose is now an employee of the US NSF; however, any opinions, findings, conclusions, or recommendations expressed in this material are those of W. G. Ambrose and his coauthors, and do not necessarily reflect the views of the US NSF. The data are stored at the Centre for Arctic Gas Hydrate, Environment and Climate data repository and are accessible by contacting giuliana.panieri@uit.no and fabio.sarti@uit.no.

References

- Aharon, P., E. R. Graber, and H. H. Roberts (1992), Dissolved carbon and 33-133-133-1 anomalies in the water column caused by hydrocarbon seeps on the northwestern Gulf of Mexico slope, *Geo Mar. Lett.*, *12*, 33–40.
- Alexis, K., J.-C. Caprais, C. Decker, M. Essirard, J. Le Bruchec, P. Noel, and K. Olu (2015), Variability in gas and solute fluxes through deep-sea chemosynthetic ecosystems inhabited by vesicomid bivalves in the gulf of Guinea, *Deep Sea Res., Part I*, *95*, 122–130, doi:10.1016/j.dsr.2014.10.01.
- Aloisi, G., et al. (2002), CH_4 -consuming microorganisms and the formation of carbonate crusts at cold seeps, *Earth Planet. Sci. Lett.*, *203*, 195–203.
- Amano, K., R. G. Jenkins, Y. Sako, M. Ohara, and S. Kiel (2013), A Paleogene deep-sea methane-seep community from Honshu, Japan, *Palaeogeogr. Palaeoclimatol. Palaeoecol.*, *387*, 126–133.
- Andresen, K. J., and M. Huuse (2011), "Bulls-eye" pockmarks and polygonal faulting in the Lower Congo Basin: Relative timing and implications for fluid expulsion during shallow burial, *Mar. Geol.*, *279*(1), 111–127.
- Archer, D., B. Buffett, and V. Brovkin (2009), Ocean methane hydrates as a slow tipping point in the global carbon cycle, *Proc. Natl. Acad. Sci. U. S. A.*, *106*(49), 20,596–20,601, doi:10.1073/pnas.0800885105.
- Bé, A. W. H., and D. S. Tolderlund (1971), Distribution and ecology of living planktonic foraminifera in surface waters of the Atlantic and Indian Oceans, in *The Micropaleontology of the Oceans*, edited by B. M. Funnell and W. R. Riedel, pp. 105–149, Cambridge Univ. Press, London, U. K.
- Benway, H. M., J. F. McManus, D. W. Oppo, and J. L. Cullen (2010), Hydrographic changes in the eastern subpolar North Atlantic during the last deglaciation, *Quat. Sci. Rev.*, *29*(23–24), 3336–3345.
- Berndt, C. (2014), Temporal constraints on hydrate-controlled methane seepage off Svalbard, *Science*, *343*, 284–287.
- Birgel, B., and H. C. Hass (2004), Oceanic and atmospheric variations during the last deglaciation in the Fram Strait (Arctic Ocean): A coupled high-resolution organic-geochemical and sedimentological study, *Quat. Sci. Rev.*, *23*, 29–47, doi:10.1016/j.quascirev.2003.10.001.
- Boetius, A., et al. (2000), A marine anaerobic consortium apparently mediating anaerobic oxidation of methane, *Nature*, *407*, 623–626.
- Bohrmann, G., J. Greinert, E. Suess, and M. Torres (1998), Authigenic carbonates from the Cascadia subduction zone and their relation to gas hydrate stability, *Geology*, *26*(7), 647–665.
- Bünz, S., S. Polyanov, S. Vadakkepullyambatta, C. Consolaro, and J. Mienert (2012), Active gas venting through hydrate-bearing sediments on the Vestnesa Ridge, offshore W-Svalbard, *Mar. Geol.*, *332–334*, 189–197, doi:10.1016/j.margeo.2012.09.012.
- Butler, P. G., A. D. Wanamaker Jr., J. D. Scourse, C. A. Richardson, and D. R. Reynolds (2011), The stability of shell $\delta^{13}\text{C}$ with respect to biological age in mature specimens of the long-lived bivalve *Arctica islandica*, *Palaeogeogr. Palaeoclimatol. Palaeoecol.*, *302*, 21–30, doi:10.1016/j.palaeo.2010.03.038.

- Callander, R., and E. N. Powell (2000), Long term history of chemoautotrophic clam dominated faunas of petroleum seeps of northwestern Gulf of Mexico, *Facies*, *43*, 177–204, doi:10.1007/BF02536990.
- Campbell, K. A. (2006), Hydrocarbon seep and hydrothermal vent paleoenvironments and paleontology: Past developments and future research directions, *Palaeogeogr. Palaeoclimatol. Palaeoecol.*, *232*, 362–407, doi:10.1016/j.palaeo.2005.06.018.
- Campbell, K. A., and D. J. Bottjer (1995), *Peregrinella*: An Early Cretaceous cold-seep-restricted brachiopod, *Paleobiology*, *24*, 461–478.
- Carmichael, R. H., T. Hattenrath, I. Valiela, and R. H. Michener (2008), Nitrogen stable isotopes in the shell of *Mercenaria mercenaria* trace wastewater inputs from watersheds to estuarine ecosystems, *Aquat. Biol.*, *4*, 99–111.
- Carroll, M. L., W. G. Ambrose, B. S. Levin, W. L. Locke, G. A. Henkes, H. Hop, and P. E. Renaud (2011), Pan-Svalbard growth rate variability and environmental regulation in the Arctic bivalve *Serripes groenlandicus*, *J. Mar. Syst.*, *88*, 239–251.
- Cavanaugh, C. M. (1983), Symbiotic chemoautotrophic bacteria in marine invertebrates from sulphide-rich habitats, *Nature*, *302*, 58–61.
- Chien, C.-W., C.-Y. Huang, C. Zhong, L. Horng-Chun, and R. Harris (2012), Miocene shallow-marine cold seep carbonate in fold-and-thrust Western Foothills, SW Taiwan, *J. Asian Earth Sci.*, *58*, 201–211.
- Consolaro, C., T. Rasmussen, G. Panieri, J. Mienert, S. Bünz, and K. Szybor (2015), Carbon isotope ($\delta^{13}\text{C}$) excursions suggest times of major methane release during the last 14 kyr in Fram Strait, the deep-water gateway to the Arctic, *Clim. Past*, *11*(4), 669–685, doi:10.5194/cp-11-669-2015.
- Craig, H. (1957), Isotopic standards for carbon and oxygen and correction factors for mass-spectrometric analysis of carbon dioxide, *Geochim. Cosmochim. Acta*, *12*, 133–149.
- Davy, B., I. Pecher, R. Wood, L. Carter, and K. Gohl (2010), Gas escape features off New Zealand: Evidence of massive release of methane from hydrates, *Geophys. Res. Lett.*, *37*, L21309, doi:10.1029/2010GL045184.
- Decker, C., K. Olu, S. Arnaud-Haond, and S. Duperron (2013), Physical proximity may promote lateral acquisition of bacterial symbionts in vesicomid clams, *PLoS ONE*, *8*(7), 1–12, doi:10.1371/journal.pone.0064830.
- Dickens, G. (2001), On the fate of past gas: What happens to methane released from a bacterially mediated gas hydrate capacitor?, *Geochem. Geophys. Geosyst.*, *2*(1), 1037, doi:10.1029/2000GC000131.
- Dickens, G. R., and M. S. Quinby-Hunt (1994), Methane hydrate stability in seawater, *Geophys. Res. Lett.*, *21*(19), 2115–2118.
- Dokken, T. M., and E. Jansen (1999), Rapid changes in the mechanism of ocean convection during the last glacial period, *Nature*, *401*(6752), 458–461.
- Dreier, A., W. Loh, M. Blumenberg, V. Thiel, D. Hause-Reitner, and M. Hoppert (2014), The isotopic biosignatures of photo- vs. thiotrophic bivalves: Are they preserved in fossil shells?, *Geobiology*, *12*(5), 406–423, doi:10.1111/gbi.12093.
- Elverhøi, A., E. S. Andersen, T. Dokken, D. Hebbeln, R. Spielhagen, J. I. Svendsen, M. Sørflaten, A. Rørnes, M. Hald, and C. F. Forsberg (1995), The growth and decay of the Late Weichselian ice sheet in western Svalbard and adjacent areas based on provenance studies of marine sediments, *Quat. Res.*, *44*, 303–316.
- Fisher, R. E., et al. (2011), Arctic methane sources: Isotopic evidence for atmospheric inputs, *Geophys. Res. Lett.*, *38*, L21803, doi:10.1029/2011GL049319.
- Gaillard, C., M. Rio, Y. Rolin, and M. Roux (1992), Fossil chemosynthetic communities related to vents or seeps in sedimentary basins: The pseudobioherms of southeastern France compared to other world examples, *Palaios*, *7*, 451–465.
- Gentz, T., E. Damm, J. S. S. von Deimling, S. Mau, D. F. McGinnis, and M. Schlüter (2014), A water column study of methane around gas flares located at the West Spitsbergen continental margin, *Cont. Shelf Res.*, *72*, 107–118.
- Graves, C. A., L. Steinle, G. Rehder, H. Niemann, D. P. Connelly, D. Lowry, R. E. Fisher, A. W. Stott, H. Sahling, and R. H. James (2015), Fluxes and fate of dissolved methane released at the seafloor at the landward limit of the gas hydrate stability zone offshore western Svalbard, *J. Geophys. Res. Oceans*, *120*, 6185–6201, doi:10.1002/2015JC011084.
- Greiner, J., G. Bohrmann, and E. Suess (2001), Gas hydrate-associated carbonates and methane-venting at Hydrate Ridge: Classification, distribution, and origin of authigenic lithologies, in *Natural Gas Hydrates: Occurrence, Distribution, and Detection*, *Geophys. Monogr. Ser.*, vol. 124, edited by C. K. Paull and P. W. Dillon, pp. 99–113, AGU, Washington, D. C.
- Grousset, F. E., E. Cortijo, S. Huon, L. Hervé, T. Richter, D. Burdloff, J. Duprat, and O. Weber (2001), Zooming in on Heinrich layers, *Paleoceanography*, *16*(3), 240–259.
- Gulin, S. B., G. G. Polikarpov, and V. N. Egorov (2003), The age of microbial carbonate structures grown at methane seeps in the Black Sea with an implication of dating of the seeping methane, *Mar. Chem.*, *84*, 67–72.
- Hald, M., and P. I. Steinsund (1996), Benthic foraminifera and carbonate dissolution in the surface sediments of the Barents and Kara Sea, *Ber. Zur Polarforschung*, *212*, 285–307.
- Han, X., E. Suess, V. Liebetrau, A. Eisenhauer, and Y. Huang (2014), Past methane release events and environmental conditions at the upper continental slope of the South China Sea: Constraints by seep carbonates, *Int. J. Earth Sci.*, *103*(7), 1873–1887, doi:10.1007/s00531-014-1018-5.
- Hein, J. R., W. R. Normark, B. R. McIntyre, T. D. Lorenson, and C. L. Powell II (2006), Methanogenic calcite, ^{13}C -depleted bivalve shells, and gas hydrate from a mud volcano offshore southern California, *Geology*, *34*, 109–112.
- Hemleben, C., M. Spindler, and O. R. Anderson (1989), *Modern Planktic Foraminifera*, Springer, N. Y.
- Hoehler, T. M., M. J. Alperin, D. B. Albert, and C. S. Martens (1994), Field and laboratory studies of methane oxidation in an anoxic marine sediment: Evidence for a methanogenic-sulfate reducer consortium, *Global Biogeochem. Cycles*, *8*(4), 451–463.
- Hornbach, M. J., N. L. Bangs, and C. Berndt (2012), Detecting hydrate and fluid flow from bottom simulating reflector depth anomalies, *Geology*, *40*, 227–230.
- Hunter, S. J., D. S. Goldobin, A. M. Haywood, A. Ridgwell, and J. G. Rees (2013), Sensitivity of the global submarine hydrate inventory to scenarios of future climate change, *Earth Planet. Sci. Lett.*, *367*, 105–115.
- Hustoft, S., S. Bünz, J. Mienert, and S. Chand (2009), Gas hydrate reservoir and active methane venting province in sediments on 20 Ma young oceanic crust in the Fram Strait, offshore NW-Svalbard, *Earth Planet. Sci. Lett.*, *284*, 12–24.
- Jansen, E., H. P. Sejrup, T. Fjaeran, M. Hald, H. Høltedahl, and O. Skarbø (1983), Late Weichselian paleoceanography of the southeastern Norwegian Sea, *Nor. Geol. Tidsskr.*, *63*, 117–146.
- Jennings, A. E., N. J. Weiner, G. Helgadottir, and J. T. Andrews (2004), Modern foraminiferal faunas of the southwestern to northern Iceland shelf: Oceanographic and environmental control, *J. Foraminiferal Res.*, *34*, 180–207.
- Jessen, S. P., T. L. Rasmussen, T. Nielsen, and A. Solheim (2010), A new Late Weichselian and Holocene marine chronology for the western Svalbard slope 30,000–0 cal years BP, *Quat. Sci. Rev.*, *29*, 1301–1312.
- Johannessen, T., E. Jansen, A. Flatøy, and A. C. Ravelo (1994), The relationship between surface water masses, oceanographic fronts and paleoclimatic proxies in surface sediments of the Greenland, Iceland, Norwegian Seas, in *Carbon Cycling in the Glacial Ocean: Constraints on the Ocean's Role in Global Change*, NATO ASI Ser., vol. 17, pp. 61–86, Springer, Berlin.

- Johnson, J. E., J. Mienert, A. Plaza-Faverola, S. Vadakkepuliambatta, J. Knies, S. Bünz, K. Andreassen, and B. Ferré (2015), Abiotic methane from ultraslow-spreading ridges can charge Arctic gas hydrates, *Geology*, *43*(5), 371–374, doi:10.1130/G36440.1.
- Kiel, S. (2010), On the potential generality of depth-related ecologic structure in cold-seep communities: Cenozoic and Mesozoic examples, *Palaeogeogr. Palaeoclimatol. Palaeoecol.*, *295*, 245–257.
- Kiel, S., and C. T. S. Little (2006), Cold-seep molluscs are older than the general marine mollusc fauna, *Science*, *313*, 1429–1431.
- King, L. H., and B. MacLean (1970), Pockmarks on the Scotian Shelf, *Geol. Soc. Am. Bull.*, *81*, 3141–3148.
- Koç, N., E. Jansen, and H. Hafliðason (1993), Paleooceanographic reconstructions of surface ocean conditions in the Greenland, Iceland and Norwegian Seas through the last 14 ka based on diatom, *Quat. Sci. Rev.*, *12*, 115–140.
- Krylova, E. M., and H. Sahling (2006), Recent bivalve molluscs of the genus *Calyptogena* (Vesicomidae), *J. Molluscan Stud.*, *72*, 359–395.
- Krylova, E. M., and H. Sahling (2010), Vesicomidae (Bivalvia): Current taxonomy and distribution, *PLoS ONE*, *5*(4), e9957, doi:10.1371/journal.pone.0009957.
- Krylova, E. M., A. V. Gebruk, D. A. Portnova, C. Todt, and H. Hafliðason (2011), New species of the genus *Isorropodon* (Bivalvia: Vesicomidae: Pliocardiinae) from cold methane seeps at Nyegga (Norwegian Sea, Vøring Plateau, Storrega Slide), *J. Mar. Biol. Assoc. U. K.*, *91*, 1135–1144.
- Lartaud, F., L. Emmanuel, M. de Rafelis, S. Pouvreau, and M. Renard (2010), Influence of food supply on the $\delta^{13}\text{C}$ signature of mollusk shells: Implications for paleoenvironmental reconstructions, *Geo Mar. Lett.*, *30*, 23–34.
- Levin, L. A. (2005), Ecology of cold seep sediments: Interactions of fauna with flow, chemistry and microbes, *Oceanogr. Mar. Biol. Annu. Rev.*, *43*, 1–46.
- Levin, L. A., and R. H. Michener (2002), Isotopic evidence for chemosynthesis-based nutrition of macrobenthos: The lightness of being at Pacific methane seeps, *Limnol. Oceanogr.*, *47*, 1336–1345, doi:10.4319/lo.2002.47.5.1336.
- Lietard, C., and C. Pierre (2008), High-resolution isotopic records ($\delta^{18}\text{O}$ and $\delta^{13}\text{C}$) and cathodoluminescence study of lucinid shells from methane seeps of the Eastern Mediterranean, *Geo Mar. Lett.*, *28*, 195–203.
- Lietard, C., and C. Pierre (2009), Isotopic signatures ($\delta^{18}\text{O}$ and $\delta^{13}\text{C}$) of bivalve shells from cold seeps and hydrothermal vents, *Geobios*, *42*, 209–219.
- Loeblich, A. R., and H. Tappan (1987), *Foraminiferal Genera and Their Classification*, vol. 1–2, Van Nostrand Reinhold, N. Y.
- Luff, W., and K. Wallmann (2003), Fluid flow, methane fluxes, carbonate precipitation and biogeochemical turnover in gas hydrate-bearing sediments at Hydrate Ridge, Cascadia Margin: Numerical modeling and mass balances, *Geochim. Cosmochim. Acta*, *67*, 3403–3421.
- MacDonald, G. (1990), Role of methane clathrates in past and future climates, *Clim. Change*, *16*, 247–281.
- Mackensen, A., and M. Hald (1988), *Cassidulina teretis* Tappan and *C. laevigata* d'Orbigny: Their modern and Late Quaternary distribution in northern seas, *J. Foraminiferal Res.*, *18*, 16–24.
- Mae, A., T. Yamanaka, and S. Shimoyama (2007), Stable isotope evidence for identification of chemosynthesis-based fossil bivalves associated with cold-seepages, *Palaeogeogr. Palaeoclimatol. Palaeoecol.*, *245*, 411–420.
- Majima, R., T. Nobuhara, and T. Kitazaki (2005), Review of fossil chemosynthetic assemblages in Japan, *Palaeogeogr. Palaeoclimatol. Palaeoecol.*, *227*, 86–123, doi:10.1016/j.palaeo.2005.04.028.
- Mangerud, J., and S. Gulliksen (1975), Apparent radiocarbon ages of recent marine shells from Norway, Spitsbergen, and Arctic Canada, *Quat. Res.*, *5*(2), 263–273, doi:10.1016/0033-5894(75)90028-9.
- Mangerud, J., S. Bondevik, S. Gulliksen, A. Hufthammer, and T. Høisæter (2006), Marine ^{14}C reservoir ages for 19th century whales and molluscs from the North Atlantic, *Quat. Sci. Rev.*, *25*, 3228–3245.
- Marin-Moreno, H., T. A. Minshull, G. K. Westbrook, B. Sinha, and S. Sarkar (2013), The response of methane hydrate beneath the seabed offshore Svalbard to ocean warming during the next three centuries, *Geophys. Res. Lett.*, *40*, 5159–5163, doi:10.1002/grl.50985.
- Mattingsdal, R., J. Knies, K. Andreassen, K. Fabian, K. Husum, K. Grøsfjeld, and S. De Schepper (2014), A new 6 Myr stratigraphic framework for the Atlantic–Arctic Gateway, *Quat. Sci. Rev.*, *92*, 170–178.
- McConnaughey, T. A., and D. P. Gillikin (2008), Carbon isotopes in mollusk shell carbonates, *Geo Mar. Lett.*, *28*, 287–299.
- McConnaughey, T. A., J. Burdett, J. F. Whelan, and C. K. Paull (1997), Carbon isotopes in biological carbonates: Respiration and photosynthesis, *Geochim. Cosmochim. Acta*, *61*, 611–622.
- Mienert, J. (2013), *CAGE Cruise Report for 08 October 2013–25 October 2013 on Board the FF Helmer Hanssen*, 42 pp., The Arctic University of Tromsø, Tromsø, Norway.
- Mienert, J., M. Vanneste, S. Bünz, K. Andreassen, H. Hafliðason, and H. P. Sejrup (2005), Ocean warming and gas hydrate stability on the mid-Norwegian margin at the Storegga Slide, *Mar. Pet. Geol.*, *22*, 233–244.
- Millo, C., M. Sarnthein, H. Erlenkeuser, and T. Frederichs (2005), Methane-driven late Pleistocene $\delta^{13}\text{C}$ minima and overflow reversals in the southwestern Greenland Sea, *Geology*, *33*, 873–876.
- Müller, J., and R. Stein (2014), High-resolution record of late glacial and deglacial sea ice changes in Fram Strait corroborates ice–ocean interactions during abrupt climate shifts, *Earth Planet. Sci. Lett.*, *403*, 446–455.
- Nedoncelle, K., N. LeBris, M. de Rafelis, N. Labourdette, and F. Lartaud (2014), Non-equilibrium fractionation of stable carbon isotopes in chemosynthetic mussels, *Chem. Geol.*, *387*, 35–46.
- Niemann, H., et al. (2006), Novel methanotrophic communities of the Haakon Mosby mud volcano and their role as methane sink, *Nature*, *443*, 854–858.
- Nørgaard-Pedersen, N., R. F. Spielhagen, H. Erlenkeuser, P. M. Grootes, J. Heinemeier, and J. Knies (2003), Arctic Ocean during the Last Glacial Maximum: Atlantic and polar domains of surface water mass distribution and ice cover, *Paleoceanography*, *18*(3), 1063, doi:10.1029/2002PA000781.
- O'Donnell, T. H., S. A. Macko, J. Chou, K. L. Davis-Hartten, and J. F. Wehmiller (2003), Analysis of $\delta^{13}\text{C}$, $\delta^{15}\text{N}$, and $\delta^{34}\text{S}$ in organic matter from the biominerals of modern and fossil *Mercenaria* spp., *Org. Geochem.*, *34*, 165–183.
- Owen, E. F., A. D. Wanamaker, S. C. Feindel, B. R. Schöne, and P. D. Rawson (2008), Stable carbon and oxygen isotope fractionation in bivalve (*Placopecten magellanicus*) larval aragonite, *Geochim. Cosmochim. Acta*, *72*, 4687–4698.
- Panieri, G., A. Camerlenghi, S. Conti, G. A. Pini, and I. Cacho (2009), Methane seepages recorded in benthonic foraminifera from Miocene seep carbonates, Northern Apennines (Italy), *Palaeogeogr. Palaeoclimatol. Palaeoecol.*, *284*, 271–282.
- Panieri, G., R. H. James, A. Camerlenghi, G. K. Westbrook, C. Consolaro, I. Cacho, V. Cesari, and C. S. Cervera (2014), Record of methane emissions from the West Svalbard continental margin during the last 23,500 yrs. revealed by $\delta^{13}\text{C}$ of benthic foraminifera, *Global Planet. Clim. Change*, *122*, 151–160.
- Paull, C. K., C. S. Martens, J. P. Chanton, A. C. Neumann, J. Coston, A. J. T. Jull, and L. J. Toolin (1989), Old carbon in living organisms and young CaCO_3 cements from abyssal brine seeps, *Nature*, *342*, 166–168.

- Paull, C. K., W. R. Normak, W. Ussler III, D. W. Caress, and R. Keaten (2008), Association among active seafloor deformation, mound formation, and gas hydrate growth and accumulation within the seafloor of the Santa Monica Basin, offshore California, *Mar. Geol.*, *250*, 258–275.
- Peckmann, J., O. H. Walliser, W. Reigel, and J. Reitner (1999), Signatures of hydrocarbon venting in a middle Devonian carbonate mound (Hollard Mound) at the Hamar Laghdad (AntiAtlas, Morocco), *Facies*, *40*, 281–296.
- Peckmann, J., A. Reimer, C. Luth, B. T. Hansen, C. Heinicke, J. Hoefs, and J. Reitner (2001), Methane-derived carbonate and authigenic pyrite from the northwestern Black Sea, *Mar. Geol.*, *177*(1–2), 129–150.
- Peersen, R. (2006), Sedimentary processes on the SvalbardeBarents Sea continental margin and glacial history of the Storfjorden area from the LGM through the Early Holocene, MS thesis, Dep. Earth Sci., Univ. Bergen, Bergen, Norway.
- Pierre, C., M.-M. Blanc-Valleron, J. Demange, O. Boudouma, J.-P. Foucher, T. Pape, T. Himmler, N. Fekete, and V. Spiess (2012), Authigenic carbonates from active methane seeps offshore southwest Africa, *Geo Mar. Lett.*, *32*, 501–513, doi:10.1007/s00367-012-0295-x.
- Plaza-Faverola, A., S. Bünz, and J. Mienert (2011), Repeated fluid expulsion through sub-seabed chimneys offshore Norway in response to glacial cycles, *Earth Planet. Sci. Lett.*, *305*(3–4), 297–308.
- Plaza-Faverola, A., S. Bünz, J. E. Johnson, S. Chand, J. Knies, J. Mienert, and P. Franek (2015), Role of tectonic stress in seepage evolution along the gas hydrate-charged Vestnesa Ridge, Fram Strait, *Geophys. Res. Lett.*, *42*, 733–742, doi:10.1002/2014GL062474.
- Rasmussen, T. L., E. Thomsen, M. A. Ślubowska, S. Jessen, A. Solheim, and N. Koç (2007), Paleocyanographic evolution of the SW Svalbard margin (76°N) since 20,000 ¹⁴C yr BP, *Quat. Res.*, *67*, 100–114, doi:10.1016/j.yqres.2006.07.002.
- Reagan, M. T., and G. J. Moridis (2007), Oceanic gas hydrate instability and dissociation under climate change scenarios, *Geophys. Res. Lett.*, *34*, L22709, doi:10.1029/2007GL031671.
- Reeburgh, W. A. (2007), Ocean marine biogeochemistry, *Chem. Rev.*, *107*, 486–513, doi:10.1021/cr050362v.
- Reimer, P. J., et al. (2013), Intcal13 and Marine13 radiocarbon age calibration curves 0–50,000 years cal bp, *Radiocarbon*, *55*(4), 1869–1887.
- Riboulot, V., Y. Thomas, S. Berné, G. Jouet, and A. Cattaneo (2014), Control of Quaternary sea level changes on gas seeps, *Geophys. Res. Lett.*, *41*, 4970–4977, doi:10.1002/2014GL060460.
- Ritger, S., B. Carson, and E. Suess (1987), Methane-derived authigenic carbonates formed by subduction-induced pore-water expulsion along Oregon/Washington margin, *Geol. Soc. Am. Bull.*, *98*, 147–156.
- Roberts, S. J., and J. Nunn (1995), Episodic fluid expulsion from geopressed sediments: Marine and Petroleum, *Geology*, *12*(2), 195–204.
- Roberts, S. J., J. Nunn, L. M. Cathles, and F. Cipriani (1996), Expulsion of abnormally pressured fluids along faults, *J. Geophys. Res.*, *101*(B12), 28,228–28,252.
- Ruppel, P. (2011), Methane hydrates and contemporary climate change, *Nat. Educ. Knowl.*, *3*, 29.
- Sahling, H., et al. (2014), Gas emissions at the continental margin west off Svalbard: Mapping, sampling, and quantification, *Biogeosciences*, *11*, 7189–7234, doi:10.5194/bg-11-7189-2014.
- Sarnthein, M., S. Van Kreveld, H. Erlenkeuser, P. M. Grootes, M. Kucera, U. Pflaumann, and M. Schulz (2003), Centennial-to-millennial-scale periodicities of Holocene climate and sediment injections off the western Barents shelf, 75°N, *Boreas*, *32*, 447–461, doi:10.1111/j.1502-3885.2003.tb01227.x.
- Sibson, R. H. (1996), Structural permeability of fluid-driven fault-fracture meshes, *J. Struct. Geol.*, *18*(8), 1031–1042.
- Simstich, J., M. Sarnthein, and H. Erlenkeuser (2003), Paired $\delta^{18}\text{O}$ signals of *N. pachyderma* (s) and *T. quinqueloba* show thermal stratification structure in the Nordic seas, *Mar. Micropaleontol.*, *48*, 107–125.
- Sloan, E. D., and C. A. Koh (2008), *Clathrate Hydrates of Natural Gases*, CRC, Boca Raton, Fla.
- Smith, A. J., J. Mienert, S. Bünz, and J. Greinert (2014), Thermogenic methane injection via bubble transport into the upper Arctic Ocean from the hydrate-charged Vestnesa Ridge, Svalbard, *Geochem. Geophys. Geosyst.*, *15*, 1945–1959, doi:10.1002/2013GC005179.
- Stabell, B. (1986), A diatom maximum horizon in upper Quaternary deposits, *Geol. Rundsch.*, *75*(1), 175–184.
- Stewart, I. S., J. Sauber, and J. Rose (2000), Glacio-seismotectonics: Ice sheets, crustal deformation and seismicity, *Quat. Sci. Rev.*, *19*, 1367–1389.
- Stuiver, M., P. J. Reimer, and R. Reimer (2014), *CALIB Radiocarbon Calibration Execute, Version 7.0html*. [Available at <http://calib.qub.ac.uk/calib/>]
- Taviani, M., L. Angeletti, and A. Ceregato (2011), Chemosynthetic bivalves of the family Solemyidae (Bivalvia, Protobranchia) in the Neogene of the Mediterranean Basin, *J. Paleontol.*, *85*, 1067–1076, doi:10.1666/10-119.1.
- Taylor, J. D., and E. A. Glover (2010), Chemosynthetic bivalves, in *The Vent and Seep Biota, Top. Geobiol.*, vol. 33, edited by S. Kiel, pp. 107–155, Springer Science and Business Media B.V., Berlin, Germany.
- Thiel, V., J. Peckmann, R. Seifert, P. Wehrung, J. Reitner, and W. Michaelis (1999), Highly isotopically depleted isoprenoids: Molecular markers for ancient methane venting, *Geochim. Cosmochim. Acta*, *63*, 3959–3966.
- Thurber, A. R., K. Kroger, C. Neira, H. Wiklund, and L. A. Levin (2010), Stable isotope signatures and methane use by New Zealand cold seep benthos, *Mar. Geol.*, *272*, 260–269, doi:10.1016/j.margeo.2009.06.001.
- Thurber, A. R., L. A. Levin, A. A. Rowden, S. Sommer, P. Linke, and K. Kröger (2013), Microbes, macrofauna, and methane: A novel seep community fueled by aerobic methanotrophy, *Limnol. Oceanogr. Methods*, *58*, 1640–1656, doi:10.4319/lo.2013.58.5.1640.
- Torres, M. E., J. P. Barry, D. A. Hubbard, and E. Suess (2001), Reconstructing the history of fluid flow at cold seep sites from Ba/Ca in vesicomyid clam shells, *Limnol. Oceanogr.*, *46*, 1701–1708.
- Torres, M. E., A. C. Mix, K. Kinports, B. Haley, G. P. Klinkhammer, J. McManus, and M. A. de Angelis (2003), Is methane venting at the seafloor recorded by $\delta^{13}\text{C}$ of benthonic foraminifera shells?, *Paleoceanography*, *18*(3), 1062, doi:10.1029/2002PA000824.
- Torres, M. E., R. A. Martin, G. P. Klinkhammer, and E. Nesbitt (2010), Post depositional alteration of foraminiferal shells in cold seep settings: New insights from flow-through time-resolved analysis of biogenic and inorganic seep carbonates, *Earth Planet. Sci. Lett.*, *299*, 10–22.
- Treude, T., A. Boetius, K. Knittel, K. Wallmann, and B. B. Jørgensen (2003), Anaerobic oxidation of methane above gas hydrates (Hydrate Ridge, OR), *Mar. Ecol. Prog. Ser.*, *264*, 1–14.
- Van Dover, C. L. (2000), *The Ecology of Deep-Sea Hydrothermal Vents*, 448 pp., Princeton Univ. Press, Princeton, N. J.
- Van Dover, C. L. (2007), Stable isotope studies in marine chemoautotrophically based ecosystems: An update, in *Stable Isotopes in Ecology and Environmental Science*, vol. 2, edited by R. Michener and K. Lajtha, pp. 202–237, John Wiley, Hoboken, N. J.
- Vanreusel, A., et al. (2009), Biodiversity of cold seep ecosystems along the European margins, *Oceanography*, *22*, 110–127.
- Volkman, R., and M. Mensch (2001), Stable isotope composition ($\delta^{18}\text{O}$, $\delta^{13}\text{C}$) of living planktic foraminifers in the outer Laptev Sea and the Fram Strait, *Mar. Micropaleontol.*, *42*, 163–188.
- Westbrook, G. K., et al. (2009), Escape of methane gas from the seabed along the West Spitsbergen continental margin, *Geophys. Res. Lett.*, *36*, L15608, doi:10.1029/2009GL039191.